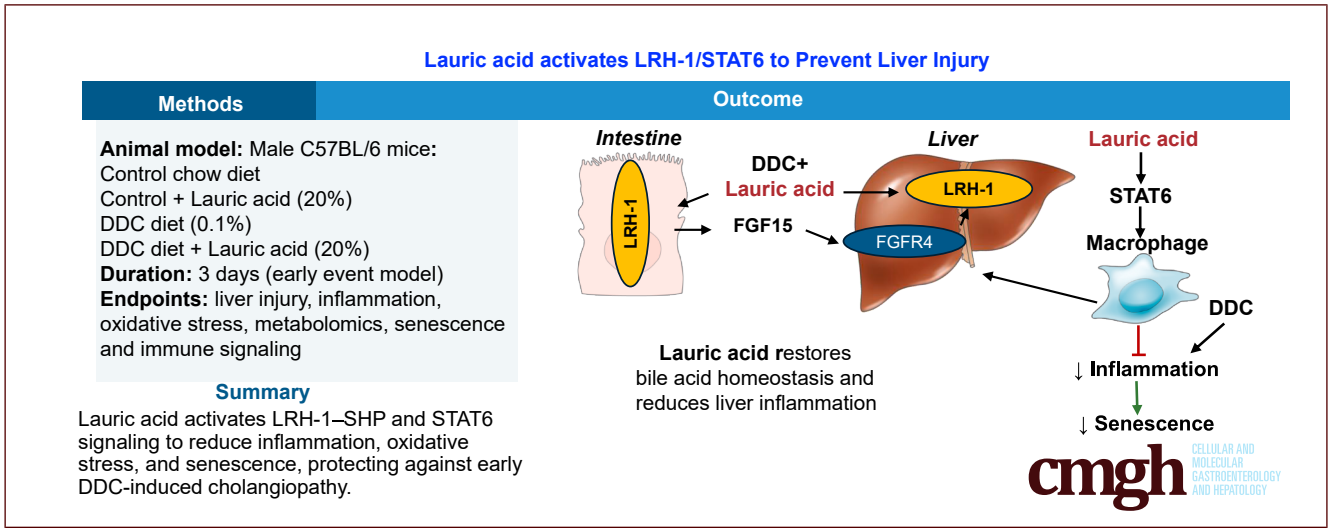
cmgh
CELLULAR AND MOLECULAR GASTROENTEROLOGY AND HEPATOLOGY

ORIGINAL RESEARCH

Dietary Lauric Acid Suppresses Inflammation, Cholestasis, Hepatocyte Injury, and Senescence in 3,5-Diethoxycarbonyl-1,4-Dihydrocollidine-induced Inflammatory Cholangiopathy

Swati Ghosh,[1] Michael W. Devereaux,[1] Aimee L. Anderson,[1] Colin C. Anderson,[2] Angelo D'Alessandro,[2] David J. Orlicky,[3] and Ronald J. Sokol[1,4]

[1]Department of Pediatrics, University of Colorado School of Medicine, Aurora, Colorado; [2]Department of Biochemistry and Molecular Genetics, University of Colorado School of Medicine, Aurora, Colorado; [3]Department of Pathology, University of Colorado School of Medicine, Aurora, Colorado; and [4]Digestive Health Institute, Children's Hospital Colorado, Aurora, Colorado



SUMMARY

Lauric acid protects against cholestatic liver injury in a mouse model by restoring bile acid balance, reducing oxidative stress, suppressing senescence, and modulating immune signaling, highlighting its potential as a therapy for inflammatory cholangiopathies and bile acid-induced liver dysfunction.

WHAT YOU NEED TO KNOW

Background: Inflammatory cholangiopathies currently lack effective therapies. Lauric acid (LA) is a medium chain fatty acid that can convert to the liver receptor homolog 1 (LRH-1) agonist dilauroylphosphatidylcholine (DLPC), which may be beneficial in these diseases.

Impact: Dietary LA in a short-term mouse model (DDC induced cholangiopathy) reduced inflammation, cholestasis, hepatocyte injury, and senescence by activating LRH-1 signaling, restoring bile acid homeostasis, and promoting anti-inflammatory macrophage polarization.

Future Directions: Future studies should analyze if LA has these beneficial effects in chronic cholangiopathy models and determine if this is a therapeutic target for human cholangiopathies.

BACKGROUND & AIMS: Inflammatory cholangiopathies involve complex hepatic cell-cell interactions, contributing to inflammation, cholestasis, oxidative stress, senescence, and bile acid dysregulation. The objective of this proof-of-principle study was to examine the early-stage effects of lauric acid (LA), a dietary fatty acid and precursor of the liver receptor homolog 1 (LRH-1) agonist dilauroylphosphatidylcholine (DLPC), in a 3,5-diethoxycarbonyl-1,4-dihydrocollidine (DDC) diet-induced cholangiopathy model.

METHODS: We employed a 3-day DDC diet in male C57/BL6 mice and supplemented it with 20% dietary LA. Liver, primary hepatocytes, and intrahepatic immune cells were analyzed for senescence, oxidative stress, and macrophage polarization.

RESULTS: DDC mice showed elevated liver chemistries, hepatic inflammation (F4/80 histochemistry), ductular reaction, and increased hepatocyte senescence markers. Using liquid chromatography-mass spectrometry metabolomics, we found that DDC liver injury was marked by increased hepatic

levels of hydrophobic bile acids and oxidative stress. LA restored bile acid homeostasis and Farnesoid X receptor-LRH-1 signaling in the liver and ileum, reduced oxidative stress, and normalized cholestasis-related gene expression in conjunction with improved liver injury, inflammation, and ductular reaction. DDC mice exhibited enhanced hepatocyte senescence (upregulated *Cdkn1a, Cdkn1b, Ccl2*) and signal transducer and activator of transcription (STAT) 1 activation, all of which were attenuated by LA. Chromatin immunoprecipitation confirmed STAT1 binding to the senescence *Cdkn1b* promoter, which was suppressed by LA. Additionally, LA enhanced LRH-1-STAT6 colocalization and signaling in bone marrow-derived macrophages from DDC mice, promoting polarization from pro-inflammatory to anti-inflammatory phenotypes, which was associated with increased STAT6 and LRH-1 activation and STAT6 promoter occupancy at anti-inflammatory genes.

CONCLUSIONS: These findings indicate the plausibility of LA's therapeutic potential in inflammatory cholangiopathies, which should be pursued in chronic cholangiopathy models. *(Cell Mol Gastroenterol Hepatol 2026;20:101731; https://doi.org/10.1016/j.jcmgh.2026.101731)*

Keywords: Biliary Atresia; Cholangiocyte; Hepatocyte; LRH-1; Primary Sclerosing Cholangitis; macrophage.

Inflammatory cholangiopathies are a group of liver diseases (including primary sclerosing cholangitis [PSC], primary biliary cholangitis [PBC], and biliary atresia) characterized by bile duct injury and inflammation, cholestasis, and hepatocellular injury, which can ultimately lead to liver failure.[1,2] A key driver of liver injury in these disorders is the retention of hydrophobic bile acids, which triggers oxidative stress, inflammation, and cellular dysfunction.[3] Currently, there are few effective medical therapies for the majority of cholangiopathies; thus, progression to fibrosis and cirrhosis is common, highlighting the need for novel targeted therapeutic interventions.[4,5]

Cell-cell communication between cholangiocytes, hepatocytes, and macrophages plays a critical role in liver homeostasis. However, cholangiocytes may undergo stress-induced changes that impair bile flow and signal other hepatic cells to promote inflammation and cholestasis.[6,7] Hepatocytes may, in turn, suffer oxidative damage due to bile acid retention and excessive reactive oxygen species (ROS) generation, and may undergo cellular senescence, which can amplify the inflammatory state. Liver macrophages may also be activated to a pro-inflammatory phenotype, further generating inflammatory mediators and promoting tissue injury.[8]

Nuclear receptors such as farnesoid X receptor (FXR) and liver receptor homolog 1 (LRH-1) are key regulators of bile acid synthesis and transport, lipid homeostasis, and inflammation. Dysregulation of these pathways has been implicated in cholestatic liver diseases, making them promising therapeutic targets.[9–13] Additionally, senescence-associated secretory phenotype (SASP) factors may contribute to chronic inflammation and fibrosis, further sustaining the disease process.[4,7,14] Thus, restoring hepatic immune balance, reducing oxidative stress, and modulating nuclear receptor signaling are potential strategies for mitigating cholangiopathies.

Lauric acid (LA), a medium-chain fatty acid found in dietary sources such as coconut oil, has been recognized for its anti-inflammatory and antioxidative properties.[15,16] Emerging evidence suggests that the LA derivative, 1,2-dilauroyl-sn-glycero-3-phosphocholine (DLPC), activates hepatic LRH-1, which can downregulate inflammatory responses with improvement of liver injury and cholestasis in parenteral nutrition-associated cholestasis (PNAC).[13] However, the effects of LA in inflammatory cholangiopathies remain unexplored.

This proof-of-principle study investigated the effects of LA supplementation in the early stages of a murine model of inflammatory cholangiopathy induced by 3,5-diethoxycarbonyl-1,4-dihydrocollidine (DDC).[17,18] We hypothesized that, if LA modulated hepatic cell-cell interactions, attenuated oxidative stress, suppressed senescence, and promoted an anti-inflammatory macrophage phenotype (via LRH-1

Abbreviations used in this paper: **β-gal, β-galactosidase; β-MCA, beta-muricholic acid; *Abcc2*, ATP-binding cassette sub-family C member 2; ALT, alanine aminotransferase; ANOVA, analysis of variance; ASBT, apical sodium-dependent bile acid transporter; AST, aspartate aminotransferase; BMDM, bone marrow-derived macrophage; BSEP, bile salt export pump; CA, cholic acid; *Ccl2*, chemokine (C-C) motif ligand 2; CDCA, chenodeoxycholic acid; *Cdkn1a*, cyclin-dependent kinase inhibitor a; *Cdkn1b*, cyclin dependent kinase inhibitor b; ChIP, chromatin immunoprecipitation; *Cyp7a1*, cholesterol 7a hydroxylase; DAB, 3,3′-diaminobenzidine; DAPI, 4′,6-diamidino-2-phenylindole; DCA, deoxycholic acid; DDC, 3,5-diethoxycarbonyl-1,4-dihydrocollidine; DLPC, dilauroylphosphatidylcholine; DMEM, Dulbecco's Modified Eagle Medium; EBSS, Earle's Balanced Salt Solution; ELISA, enzyme-linked immunosorbent assay; FBS, fetal bovine serum; *Fgf15*, fibroblast growth factor 15; FXR, Farnesoid X receptor; GCA, glycocholic acid; GCDCA, glycochenodeoxycholic acid; GDCA, glycodeoxycholic acid; GLCA, glycolithocholic acid; GUDCA, glycoursodeoxycholic acid; H&E, hematoxylin and eosin; HRP, horseradish peroxidase; IACUC, Institutional Animal Care and Use Committee; IHMC, intrahepatic mononuclear cell; I.P, intraperitoneally; KEGG, Kyoto Encyclopedia of Genes and Genomes; LA, lauric acid; LCA, lithocholic acid; LC-MS, liquid chromatography-mass spectrometry; LRH-1, liver receptor homolog 1; MRP2, multidrug resistance-associated protein 2; *Nr0b2*, nuclear receptor subfamily 0, group B, member 2; *Nr5a2*, nuclear receptor subfamily 5, group A, member 2; NTCP, sodium taurocholate cotransporting polypeptide; OD, optical density; OST-β, organic solute transporter subunit beta; OPLS-DA, orthogonal partial least squares discriminant analysis; PBC, primary biliary cholangitis; PCA, principal component analysis; PLS-DA, partial least squares discriminant analysis; PNAC, parenteral nutrition-associated cholestasis; PSC, primary sclerosing cholangitis; PVDF, polyvinylidene fluoride; qPCR, quantitative polymerase chain reaction; qRT-PCR, quantitative real-time polymerase chain reaction; ROS, reactive oxygen species; SASP, senescence-associated secretory phenotype; SDS, sodium dodecyl sulfate; SEM, standard error of the mean; SHP, small heterodimer partner; *Slc10a1*, solute carrier family 10, member 1; *Slc10a2*, solute carrier family 10, member 2; STAT1, signal transducer and activator of transcription 1; STAT6, signal transducer and activator of transcription 6; TBS, Tris-buffered saline; TCA, taurocholic acid; TCDCA, taurochenodeoxycholic acid; TDCA, taurodeoxycholic acid; TLCA, taurolithocholic acid; TMCA, tauromuricholic acid; TUDCA, tauroursodeoxycholic acid; UDCA, ursodeoxycholic acid; UHPLC-MC, ultra-high-pressure-liquid chromatography coupled to mass spectrometry; VIP, Variable Importance in Projection.**

Most current article

© 2026 The Authors. Published by Elsevier Inc. on behalf of the AGA Institute. This is an open access article under the CC BY-NC-ND license (http://creativecommons.org/licenses/by-nc-nd/4.0/).

2352-345X
https://doi.org/10.1016/j.jcmgh.2026.101731

activation) in the early stages of inflammatory cholangiopathy, it could have potential benefits during the evolution of these chronic diseases. Furthermore, using metabolomic profiling, gene expression analysis, and immune cell characterization, we aimed to elucidate the molecular mechanisms through which LA could exert its hepatoprotective effects.

Results

Administration of Dietary LA Reduces Liver Injury and Alters Gene Expression During DDC Diet-induced Inflammatory Cholangiopathy

We established an acute inflammatory cholangiopathy mouse model employing a diet (Inotiv Pharmaceutical Company) containing 0.1% DDC given ad libitum to 8-week old male C57BL/6J mice for 3 days (DDC mice).[17] A group of similar age male DDC mice also received supplementation with 20% LA in the DDC diet for 3 days. Control mice of same age and sex received chow diet (Inotiv Pharmaceutical Company) that did not contain either DDC or LA, and a fourth group of mice received the LA-supplemented diet only. The DDC mice showed evidence of increased serum aspartate aminotransferase (AST), alanine aminotransferase (ALT), total bilirubin, alkaline phosphatase, and total bile acids, which were all normalized by LA supplementation (Figure 1*A*). Histopathological analysis of liver tissue from DDC mice revealed cholestasis, periportal inflammation, and ductular reaction by hematoxylin and eosin (H&E) staining, and increased immunohistochemical CK19 staining representing bile ductular reaction and increased macrophage infiltration by F4/80 immunohistochemical staining, which were all significantly reduced in DDC/LA mice compared with DDC mice (Figure 1*B–D*).

We selected the 3-day model to capture early mechanistic changes in inflammatory cholangiopathies. Because DDC diets can acutely reduce food intake, we analyzed body and liver weights and final liver weight:body weight ratios as well as dietary intake (Table 1). DDC, LA, and DDC-LA mice showed similar lower body weights compared with chow-fed mice, and their final liver weights and liver weight:body weight ratios were similar to each other. Dietary intake was also lower in all 3 treatment groups compared with chow mice, but comparable among them. Importantly, LA supplementation did not significantly reduce DDC diet intake compared with DDC mice. Furthermore, we visually inspected liver color as a measure of hepatic DDC-derived pigment accumulation and observed comparable color between the DDC and DDC-LA groups, consistent with similar dietary intake. We also confirmed increased levels of total porphyrins in the blood of mice in the DDC groups (Figure 1*G*).

In a prior study, we reported that activation of LRH-1 by its agonist, DLPC, was protective in mice with PNAC.[13] DLPC is a phospholipid containing LA at both the sn-1 and sn-2 positions but is usually undetectable in cells under physiological conditions. However, DLPC synthesis can be upregulated in the presence of dietary LA. To test the impact of LA supplementation on DLPC production in DDC mice, we quantified hepatic DLPC levels using liquid chromatography-mass spectrometry (LC-MS)[19–21] and found that the relative abundance of hepatic DLPC was significantly increased in mice fed either the LA diet or the DDC/LA diet (Figure 1*E*). We also assessed the effect of LA supplementation on the altered expression of hepatic bile and sterol transporters in DDC mice.[12,22] DDC mice showed a reduction in hepatic mRNA expression of key bile and sterol canalicular transporters (*Abcb11*/BSEP, *Abcg5, Abcg8)*, bile acid synthesis enzymes (*Cyp7a1, Cyp8b1)*, and relevant nuclear receptors (*Nr1h4*/FXR, *Nr5a2*/LRH-1), as well as downstream targets of LRH-1 (*Nr0b2*/SHP, *Ppara*, and *Pparg)* (Figure 1*F*). LA treatment in DDC mice significantly upregulated *Abcb11*, *Abcg5*, *Abcg8*, *Nr0b2*/small heterodimer partner (SHP), and *Nr1h4*/FXR expression, whereas *Pparg* and *Cyp8b1* did not show significant changes with LA supplementation (Figure 1*F*). In summary, our findings indicate that LA supplementation in DDC mice significantly improved biochemical, histologic, and molecular markers of liver injury and cholestasis.

Effect of Lauric Acid on the Metabolomic Profile of Bile Acids in DDC Mice

Given the previously described effects of LA on genes involved in bile acid synthesis and transport, we next evaluated its impact on hepatic bile acid composition. Accordingly, we performed a detailed analysis of bile acid species in liver using LC-MS.[19–21] Principal component analysis (PCA) was initially conducted to visualize group separation in a 2D plot, which demonstrated a clear separation between the sample groups, indicating distinct differences in the metabolomic profiles associated with different diets (Figure 2*A*). This separation was most prominent between the DDC-treated group and all other groups, along PC1, whereas there was less differentiation between the DDC/LA and LA groups along PC2. When considering all analyzed bile acids, samples with similar multivariate expression profiles clustered closely together in PCA space, except for the DDC-fed cholangiopathy group, which was distinctly separated. To further refine these findings, orthogonal partial least squares discriminant analysis (OPLS-DA) was performed, which distinguished the DDC and DDC/LA groups, as well as the LA and chow groups (Figure 2*B*). In targeted bile acid metabolomics, clustering analysis of different groups revealed a significant distinction with respect to bile acid concentration within the DDC group, visualized using heatmaps (Figure 2*C*). Using a combination of Variable Importance in Projection (VIP) scores (VIP $\geq$1 indicates a significant relationship) from multivariate modeling and fold change ($P < .05$), we identified key bile acids that were differentially expressed between groups (Figure 2*D*). In the DDC group, most hepatic bile acid concentrations were elevated compared with chow-fed controls, including hydrophobic chenodeoxycholic acid (CDCA) and lithocholic acid (LCA), conjugated acidic bile acids glycoursodeoxycholic acid (GUDCA), glycocholic acid (GCA), tauroursodeoxycholic acid (TUDCA), and taurolithocholic acid (TLCA), ursodeoxycholic acid (UDCA), and cholic acid (CA). (Figure 2*D*). Conversely, bile

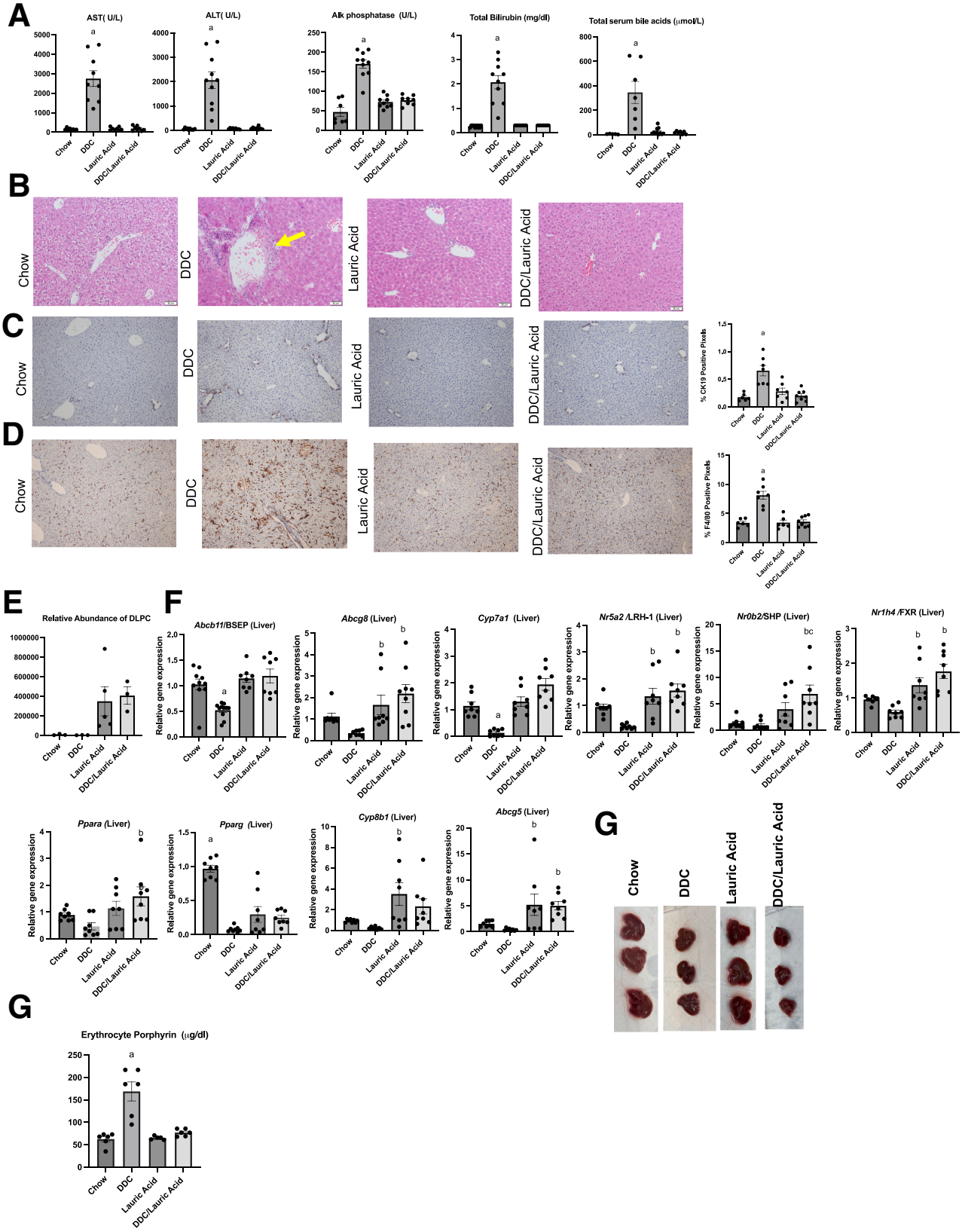

A
AST(U/L)
ALT(U/L)
Alk phosphatase (U/L)
Total Bilirubin (mg/dl)
Total serum bile acids (μmol/L)
Chow
DDC
Lauric Acid
DDC/Lauric Acid
B
C
% CK19 Positive Pixels
D
% F4/80 Positive Pixels
E
Relative Abundance of DLPC
F
Abcb11/BSEP (Liver)
Abcg8 (Liver)
Cyp7a1 (Liver)
Nr5a2 /LRH-1 (Liver)
Nr0b2/SHP (Liver)
Nr1h4 /FXR (Liver)
Ppara (Liver)
Pparg (Liver)
Cyp8b1 (Liver)
Abcg5 (Liver)
Relative gene expression
G
Erythrocyte Porphyrin (μg/dl)

Table 1. Liver, Body Weight, and Diet Intake by Mouse Group

Body weight (*g*)	Chow (n = 10)	DDC (n = 10)	LA (n = 13)	DDC/LA (n = 11)
Initial	22.8 ± 0.33	23.7 ± 0.45	22.2 ± 0.44	22.2 ± 0.35
Final	24.4 ± 0.66	21.9 ± 0.55	20.1 ± 0.48	19.4 ± 0.51
Liver weight, *g*	1.28 ± 0.08[a]	0.97 ± 0.05	0.76 ± 0.03	0.79 ± 0.04
Liver weight/final body weight ratio	0.052 ± 0.003	0.044 ± 0.002	0.038 ± 0.002[c]	0.040 ± 0.001[c]
Diet intake, gm per day per mouse	n = 5 2.30 ± 0.20	n = 6 4.16 ± 1.57	n = 6 2.17 ± 1.34	n = 6 3.25 ± 1.05

NOTE. Values are presented as mean ± standard error of the mean.
DDC, 3,5-diethoxycarbonyl-1,4-dihydrocollidine; LA, lauric acid.
[a]Significantly different from all other groups; $P < .05$.
[c]Significantly different from chow; $P < .05$.

acid concentrations were significantly reduced in DDC/LA mice compared wotj DDC mice, including hydrophobic bile acids (LCA) and beta-muricholic acid (β-MCA), and conjugated acidic bile acids taurocholic acid (TCA), taurochenodeoxycholic acid (TCDCA), TLCA, GCA, GUDCA, glycolithocholic acid (GLCA), glycochenodeoxycholic acid (GCDCA), and glycodeoxycholic acid (GDCA) (Figure 2*D*).

Next, we performed partial least squares discriminant analysis (PLS-DA) of the bile acid metabolomics data to assess sample clustering and identify key metabolites contributing to experimental group separation. Metabolite importance was determined using VIP scores and the weighted sum of absolute regression coefficients. The colored boxes in the corresponding plots indicate the relative concentrations of each metabolite across groups. We first conducted a PLS-DA between DDC and chow mice to determine the major metabolic differences. This analysis revealed that hepatic concentrations of TCDCA, TCA, TUDCA, tauromuricholic acid (TMCA), β-MCA, and UDCA were significantly increased (VIP $\geq$1) in DDC, highlighting their role in differentiating these 2 groups (Figure 2*E* and *F*). Next, we compared DDC and DDC/LA mice. The bile acids TCDCA, TCA, TUDCA, TMCA, taurodeoxycholic acid (TDCA), GUDCA, GLCA, TLCA, and LCA were significantly increased in DDC relative to DDC/LA (VIP $\geq$1) (Figure 2*F*). These findings demonstrate distinct bile acid profiles across conditions, with key metabolites contributing to the observed differences between DDC, chow, and DDC/LA mice (Table 2).

Kyoto Encyclopedia of Genes and Genomes (KEGG) pathway enrichment analysis of the bile acid metabolomics results in liver homogenate revealed significant alterations in bile acid synthesis and metabolism pathways in the DDC group compared with chow control mice (Figure 2*G*). This analysis was performed using the set of bile acids that differed significantly between groups to identify biological pathways most strongly regulated by altered bile acid metabolism in this model, rather than to capture global metabolomic enrichment.

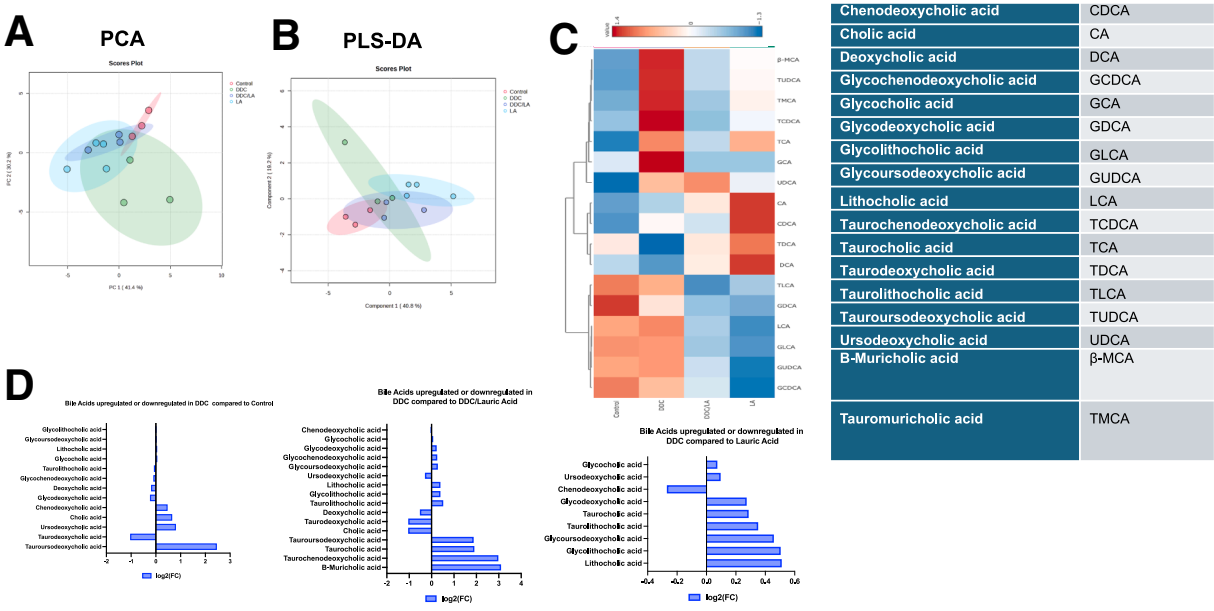
Analysis comparing DDC and DDC/LA groups demonstrated enriched pathways related to lipid metabolism, bile acid and bile salt synthesis, and biliary transport in DDC mice, which were reduced in DDC/LA mice (Figure 2*H*).

Overall, these findings suggest that treatment with LA in DDC mice results in significant shifts towards control animals in hepatic bile acid composition and concentrations, potentially mitigating cholestasis and modulating intracellular signaling pathways that regulate bile acid metabolism.

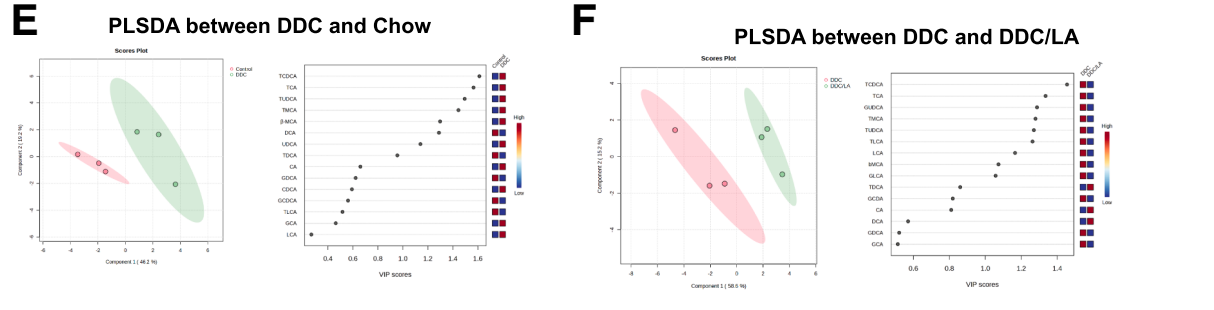
Lauric Acid Restores the Hepatocyte Expression of Bile Transporters and Promotes Bile Acid Homeostasis

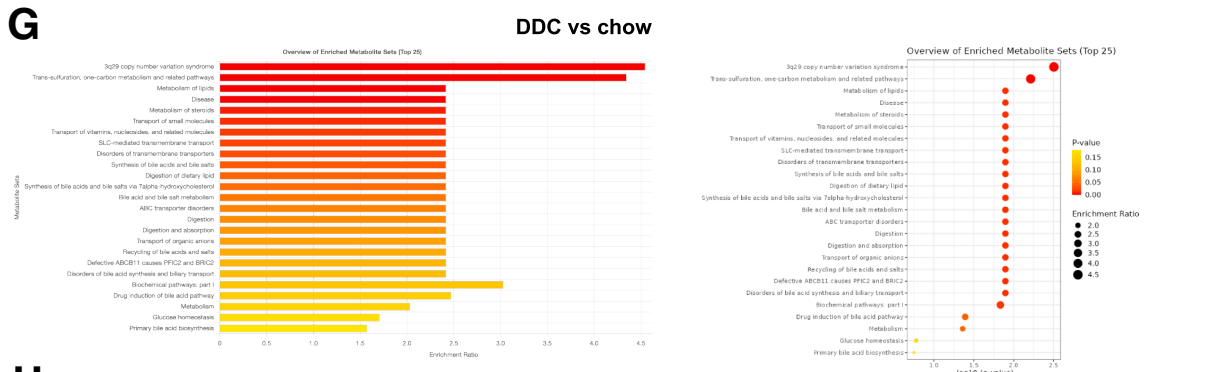
We next explored the effects of LA treatment on gene expression in hepatocytes and the terminal ileum in DDC

Figure 1. (***See previous page***). **Administration of dietary lauric acid reduces liver injury and alters gene expression during DDC diet-induced inflammatory cholangiopathy.** Mice were fed a DDC diet or chow, with or without supplementation with LA, for 3 days, and serum was obtained. (*A*) LA supplementation reduced the DDC-induced markedly elevated AST, ALT, alkaline phosphatase, total bilirubin, and total serum bile acids to near normal (chow) levels. (*B*) Liver sections stained with H&E showed evidence of cholestasis, inflammation, bile duct injury, and ductular reaction (*yellow arrow*) in DDC mice, which was prevented in DDC/LA mice. (*C*) CK19 staining of cholangiocytes further demonstrated the ductular reaction in DDC mice, which was reversed by LA. (*D*) F4/80 staining demonstrated a significant infiltration of macrophages in DDC mice, which was reduced to chow levels in DDC/LA mice. (*E*) LC-MS quantification of DLPC showed that LA supplementation enhanced the relative abundance of DLPC in the liver from the 2 groups of LA-supplemented mice. (*F*) qRT-PCR mRNA expression analysis of liver showed significant reduction in DDC mice of *Abcb11, Abcg8, Cyp7a1, Nr5a2, Nr0b2, Nr1h4*, *Ppara, PPARg, Cyp8b1,* and *Abcg5,* all of which were normalized by LA treatment. (*G*) Gross liver morphology and erythrocyte porphyrin levels in mice under different dietary conditions. Representative liver images from mice in the chow, DDC, LA, and DDC/LA groups, showing darkened color in those receiving DDC. Quantification of erythrocyte porphyrin levels in the corresponding groups. Data points represent individual mice; n = 8 animals per group, except for (*C–E*) and (*G*) (n = 5–7). Statistical analysis was performed by 1-way ANOVA with Tukey's correction for multiple comparisons. [a]$P < .05$ vs all other groups; [b]$P < .05$ vs DDC; [c]$P < .05$ vs chow.



Bile Acids	Short Form
Chenodeoxycholic acid	CDCA
Cholic acid	CA
Deoxycholic acid	DCA
Glycochenodeoxycholic acid	GCDCA
Glycocholic acid	GCA
Glycodeoxycholic acid	GDCA
Glycolithocholic acid	GLCA
Glycoursodeoxycholic acid	GUDCA
Lithocholic acid	LCA
Taurochenodeoxycholic acid	TCDCA
Taurocholic acid	TCA
Taurodeoxycholic acid	TDCA
Taurolithocholic acid	TLCA
Tauroursodeoxycholic acid	TUDCA
Ursodeoxycholic acid	UDCA
B-Muricholic acid	β-MCA
Tauromuricholic acid	TMCA





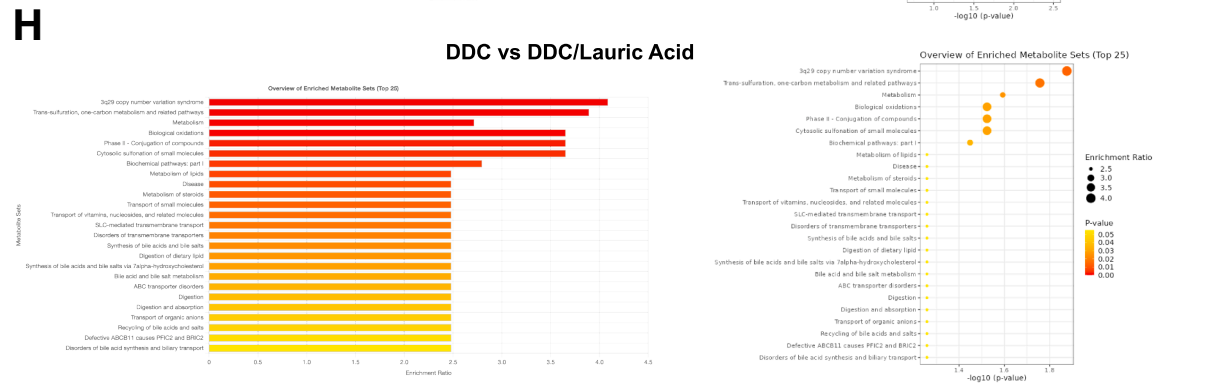


Table 2. VIP Scores for Comparison of Bile Acid Species Between Experimental Groups

Bile acids	Type	VIP	Differential expression
DDC vs control			
TMCA	Conjugated	1.3531	High in DDC
β-MCA	Un-conjugated	1.1111	High in DDC
TCA	Conjugated	1.5491	High in DDC
TCDCA	Conjugated	1.6363	High in DDC
TUDCA	Conjugated	1.426	High in DDC
TDCA	Conjugated	1.0296	Low in DDC
DDC vs DDC/LA			
TMCA	Conjugated	1.1721	High in DDC
β-MCA	Un-conjugated	0.9436	High in DDC
TCA	Conjugated	1.2884	High in DDC
TCDCA	Conjugated	1.431	High in DDC
TUDCA	Conjugated	1.1918	High in DDC
TDCA	Conjugated	0.90146	Low in DDC
CA	Un-conjugated	0.84401	Low in DDC

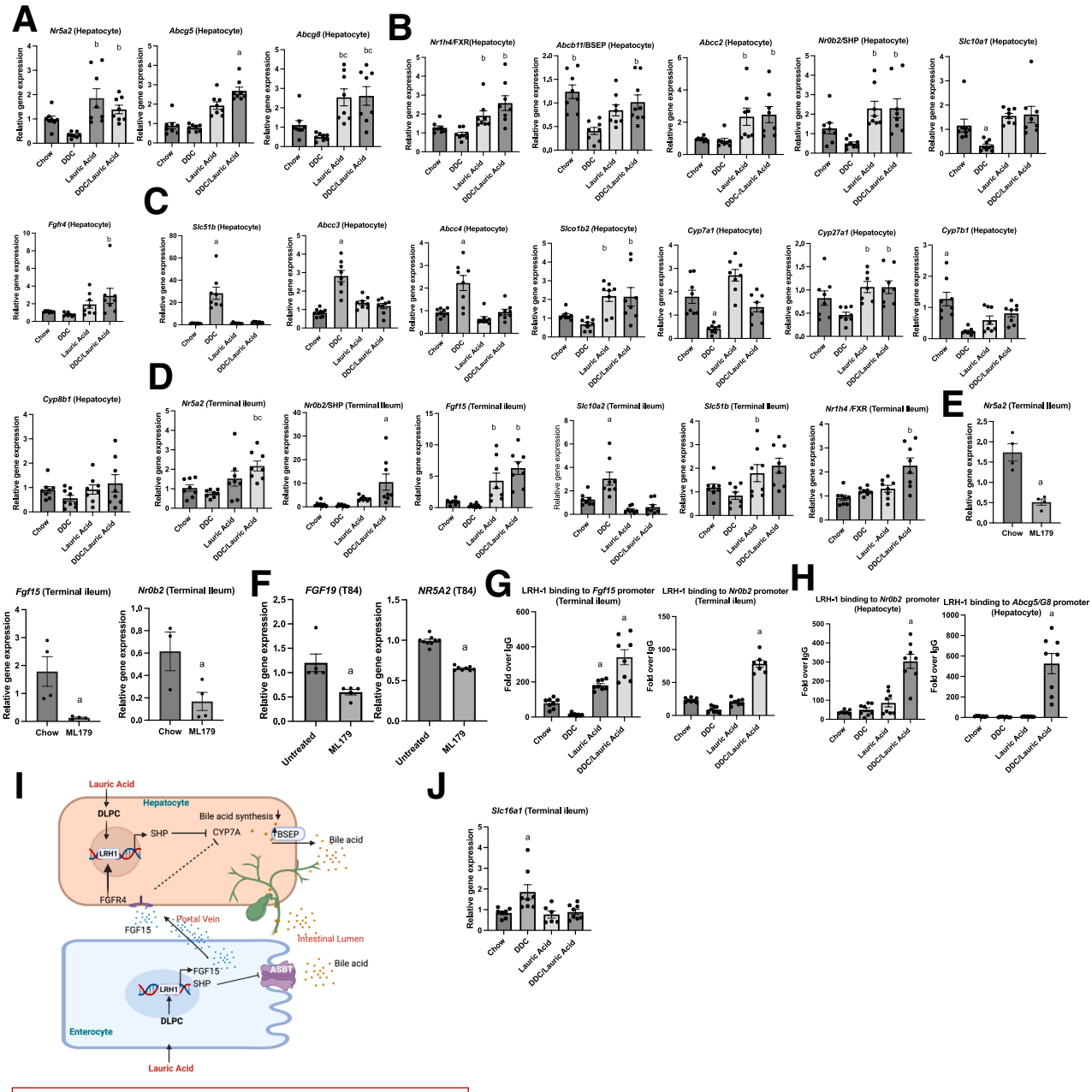
β-MCA, beta-muricholic acid; CA, cholic acid; DDC, 3,5-diethoxycarbonyl-1,4-dihydrocollidine; LA, lauric acid; TCA, taurocholic acid; TCDCA, taurochenodeoxycholic acid; TDCA, taurodeoxycholic acid; TMCA, tauromuricholic acid; TUDCA, tauroursodeoxycholic acid; VIP, Variable Importance in Projection.

mice. To understand hepatocyte-specific alterations, we first isolated primary hepatocytes from chow, DDC, LA, and DDC/LA mice and performed quantitative polymerase chain reaction (qPCR) analysis of canonical LRH-1 target genes. DDC treatment showed a trend toward reduced expression of LRH-1 target genes; however, these changes were not statistically significant compared with chow controls (Figure 3*A*). Because we previously demonstrated that LRH-1 signaling affects FXR signaling in both cultured hepatocytes and in vivo in PNAC mouse models,[12] we next investigated the effect of LA on FXR target genes in hepatocytes from DDC mice. LA treatment significantly upregulated all FXR target genes in DDC-fed mice compared with DDC alone (Figure 3*B*). In contrast, *Slc51b*/OSTB, *Abcc3*/MRP3, *and Abcc4*/MRP4 were upregulated in DDC mice, most likely to compensate for the reduced *Abcb11,* and were normalized in DDC-LA mice (Figure 3*C*). *Cyp7a1*, the rate-limiting gene for bile acid synthesis, and *Cyp7b1* were significantly suppressed by DDC, similar to other cholestatic models,[11–13] and were normalized by LA treatment (Figure 3*C*). Similar trends were noted in other bile acid synthesis genes, although the LA effect was variable (Figure 3*C*).

In the terminal ileum of DDC mice, LA treatment increased expression of *Fgf15, Nr5a2, Slc51b*/OSTβ, and *Nr0b2* and reduced that of *Slc10a2*/ASBT (Figure 3*D*). Because LA may be functioning through the effects of its metabolite DLPC, an LRH-1 agonist, we next explored the role of LRH-1 in the regulation of these genes in the terminal ileum. We employed ML179, a selective inverse agonist of LRH-1, injected intraperitoneally (I.P.) for 3 days in chow-fed mice, which led to downregulation of expression of *Nr5a2*/LRH-1 and its downstream targets *Fgf15* and *Nr0b2* in the terminal ileum (Figure 3*E*). Supporting these in vivo findings, treatment of cultured human intestinal T84 cells with 5 μM ML179 overnight similarly reduced *NR5A2* and *FGF19* expression (Figure 3*F*), supporting a direct regulatory role for LRH-1 in ileal *Fgf15/19* transcription. We next performed in-silico analysis, which identified a binding site for LRH-1 on the *Fgf15* promoter in the terminal ileum. Chromatin immunoprecipitation (ChIP) assay showed that DDC mice had reduced LRH-1 binding to *Fgf15* promoter, which was reversed by LA treatment, and was similar to the effect of LA on LRH-1 binding to the SHP promoter (Figure 3*G*). These ChIP results parallel the effects of DDC and LA on mRNA expression of *Fgf15* and *Nrob*2 in the ileum (Figure 3*D*). In addition, the decreased *Nrob2*/SHP expression observed in DDC-treated mice likely contributed, at least in part, to the increased ileal expression of *Slc10a2*/apical sodium-dependent bile acid transporter (ASBT), a key transporter involved in bile acid absorption in enterocytes. The subsequent reduction of *Slc10a2* expression to chow-fed control levels in DDC-LA mice may

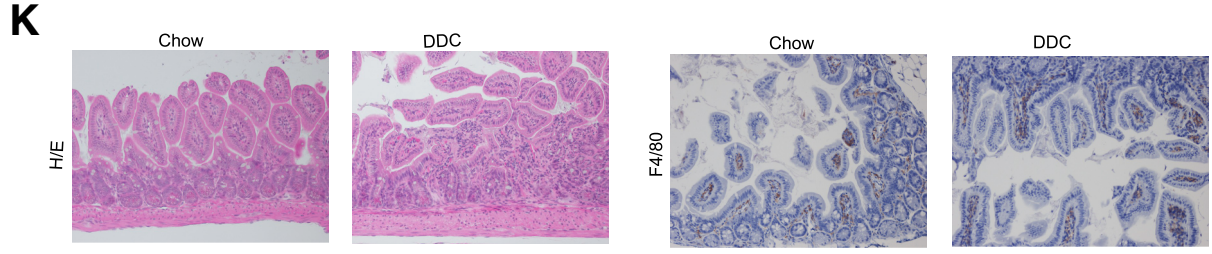
Figure 2. (***See previous page***). **Effect of LA on the metabolomic profile of liver bile acids in DDC Mice.** Targeted LC-MS metabolomics profiling of hepatic levels of bile acids. (*A*) PCA of hepatic bile acid levels shows group clustering of the 4 groups of mice. (*B*) PLS-DA of bile acid levels shows clustering by groups. (*C*) Heatmap of the normalized levels of representative hepatic bile acids segregated by group. Columns represent experimental mouse groups, and rows represent bile acid species, with the order of rows determined by hierarchical clustering (Euclidean distance, complete agglomeration method). (*D*) Fold analysis comparing bile acid levels from DDC vs chow; DDC vs DDC/LA; and DDC vs LA mouse liver. (*E* and *F*) PLS-DA and VIP to determine the major distinctions among the bile acid metabolites. Data from 3 to 4 animals per group. (*G* and *H*) Comparison of liver metabolomics pathway analysis of targeted bile acid species showing top 25 enriched metabolite sets in (*G*) DDC vs chow, or (*H*) DDC vs DDC/LA mouse liver. The level of significance between 2 groups was determined by Student's paired *t*-test. $P < .05$ was considered statistically significant.

be attributable to restored SHP activity. These data suggest that LRH-1 indirectly regulates ASBT via SHP to maintain bile acid uptake in the terminal ileum in DDC mice, which could have additive effects on promoting *Fgf15* secretion into the portal vein. We further showed that hepatic *Fgfr4* expression was upregulated in LA-DDC mice (Figure 3*B*), which has the potential to increase the expression of LRH-1[23] in the hepatocyte.



Mechanism of Lauric Acid Mediated Bile Acid Homeostasis

Created in BioRender. Ghosh, S. (2026) https://BioRender.com/z5x4rvy



To further explore the effects of LA on gene expression in the liver, we performed ChIP assays to examine LRH-1 binding to the promoter of hepatocyte *Nr0b2*. In hepatocytes from the DDC group, LRH-1 binding was significantly increased by LA treatment, consistent with LRH-1 mediating the effects of LA on hepatocyte gene expression (Figure 3*H*). The resulting elevated SHP levels could then inhibit *Cyp7A1* expression (Figure 3*C*), thereby reducing bile acid synthesis. LA treatment also increased bile salt export pump (BSEP) expression (Figure 3*B*), which would enhance bile acid export into canaliculi and reduce hepatocyte bile acid levels and their potential hepatotoxicity. We also measured binding of LRH-1 to promoters of its other target genes, *Abcg5/8,* and found that LRH-1 binding was induced in hepatocytes with LA treatment (Figure 3*H*). Taken together, our data identify LRH-1 as a key transcriptional regulator of intestinal *Fgf15/19*, acting in parallel with FXR to restore bile acid homeostasis. LA, through its metabolite DLPC, enhances this regulatory network by activating LRH-1, which may act to reduce hepatocyte bile acid retention through both ileal and hepatocyte pathways (Figure 3*I*). Additionally, the elevated *Slc16a1* expression in DDC ileum, which is a marker of intestinal inflammation, was reduced by LA treatment, suggesting that LA helps mitigate gut-related inflammation in this model of cholestasis (Figure 3*J*).[24] In this regard, H&E and F4/80 staining of the DDC mouse terminal ileum showed a mild increase in macrophage infiltration (Figure 3*K*).

Effect of LA on the Liver Metabolomic Profile in DDC Mice

To further explore the effects of LA on DDC-induced alterations of liver metabolism, we next examined the effect of LA treatment on liver global metabolomics using LC-MS.[19–21] Specifically, we focused on metabolites related to amino acids, fatty acids, nucleotides, carnitine, glycolysis, and the pentose phosphate/tricarboxylic acid cycle. Examining fold change analysis for individual metabolites, the DDC group exhibited changes in liver levels compared with chow controls of fatty acids, amino acids, carnitines, glycophospholipids, glycolysis metabolites, and tricarboxylic acid/pentose phosphate metabolites, and nucleosides, many of which were significantly reversed by LA treatment in the DDC mice (Figure 4*A*–*G*). Two-dimensional PCA plots revealed separation into three clusters with the LA and DDC/LA mice superimposed on each other and the Chow and DDC mice clustering separately (Figure 4*H*).

LA Effects on Inflammation, Senescence, Mitochondrial Dysfunction, and Oxidative Stress in DDC Mice

We previously reported that in PNAC, hepatocyte injury is associated with increased cytokine production, hepatocyte apoptosis, and suppression of FXR-LRH-1 signaling.[10,12,25,26] To determine if these processes were similarly involved in the pathogenesis of cholestasis in DDC mice, we next measured the expression of genes involved in inflammatory pathways, mitochondrial dysfunction, oxidative stress, and cellular senescence in fresh hepatocytes isolated from the 4 groups of mice. DDC mice showed significantly upregulated expression of genes (Figure 5*A* and *B*) associated with oxidative stress (*Nfe212/ Nrf2*, *Nqo1*, *Hmox1*, *Prdx2, Srebf1*), inflammation (*Il6*, *Ccl5*, *Ccl2*, *Tnf, Ccr2*), and senescence (*Cdkn1a*, *Cdkn1b,* and *Cdkn2a)*. All of these changes were reversed or normalized by LA treatment of DDC mice. Genes regulating mitochondrial function (Figure 5*C*) were variably suppressed in DDC mice but were all upregulated by LA treatment.

To further examine for evidence of senescence and oxidative stress, we isolated hepatocytes from all 4 groups, plated them overnight, and subsequently stained them for β-galactosidase (β-gal) activity, a marker of cellular senescence. β-gal-positive hepatocytes were present in DDC mice but were absent in the DDC/LA mice (Figure 5*D*). We further found increased β-galactosidase protein measured by immunoblotting in hepatocytes from DDC mice, which was significantly reduced in DDC/LA mice (Figure 5*E*). Taken together, these data suggest that LA treatment effectively mitigates senescence in hepatocytes from DDC mice. Senescent hepatocytes promote liver injury progression by

Figure 3. (***See previous page***). **LA restores the expression of sterol and bile transporters in hepatocytes or the ileum isolated from experimental mice.** qRT-PCR-mRNA analysis performed in hepatocytes isolated from chow, DDC, LA, and DDC/LA mice for (*A*) *Nr5a2, Abcg5, Abcg8*; (*B*) *Nr1h4, Abcb11, Abcc2, Nr0b2, Slc10a1,* and *Fgfr4*; and (*C*) *Slc51b, Abcc3, Abcc4, Slco1b2, Cyp7a1, Cyp27a1, Cyp8b1, and Cyp7b1*. (*D*) mRNA levels from terminal ileal tissue from chow, DDC, LA, and DDC/LA mice for *Nr5a2, Nr0b2*, *Fgf15, Slc10a2, Slc51b2,* and *Nr1h4.* (*E*) mRNA levels of *Fgf15*, *Nr5a2,* and *Nr0b2* from terminal ileum isolated from chow mice and mice injected with ML179; (*F*) T84 cells were incubated with and without ML179 overnight. mRNA expression by qPCR was measured for *FGF19* and *Nr5a2,* showing reduced mRNA expression in ML179-treated cells. (*G* and *H*) ChIP assay performed on ileal and liver homogenates for LRH-1 binding to the promoter regions of (*G*) *Fgf15* (ileum*), Nr0b2* (ileum), and (*H*) *Nr0b2* (Hepatocytes), *Abcg5/8* (hepatocytes) from chow, DDC, LA, and DDC/LA mice. (*I*) Summary figure showing the proposed mechanism of LA-derived DLPC mediated activation of LRH-1-FGF15-SHP signaling axis in bile acid homeostasis (Created with BioRender.com). LA-derived DLPC in DDC-fed mice activates the nuclear receptor LRH-1, which binds to the promoters of *Fgf15* and *Nr0b2*/SHP, upregulating their expression. Secreted intestinal FGF15 then binds to FGFR4 on hepatocytes, leading to further activation of hepatic LRH-1, which then enhances hepatic *Nr0b2*/SHP expression, which in turn interacts with and suppresses *Cyp7a1*, reducing bile acid synthesis. SHP in enterocytes is known to downregulate expression of ASBT, reducing bile acid uptake from the intestinal lumen. (*J*) mRNA levels of *Slc16a1*/MCT1 in terminal ileal tissue from chow, DDC, LA, and DDC/LA mice. (*K*) Terminal ileum histologic sections from chow and DDC mice were stained with H&E and F4/80 (macrophages), demonstrating mildly increased inflammation in DDC mouse ileum. Statistical analysis was performed by 1-way ANOVA with Tukey's correction for multiple comparisons and 2 tailed unpaired Student's t-test. $^{a}P < .05$ vs all other groups; $^{b}P < .05$ vs DDC. $^{c}P < .05$ vs chow.

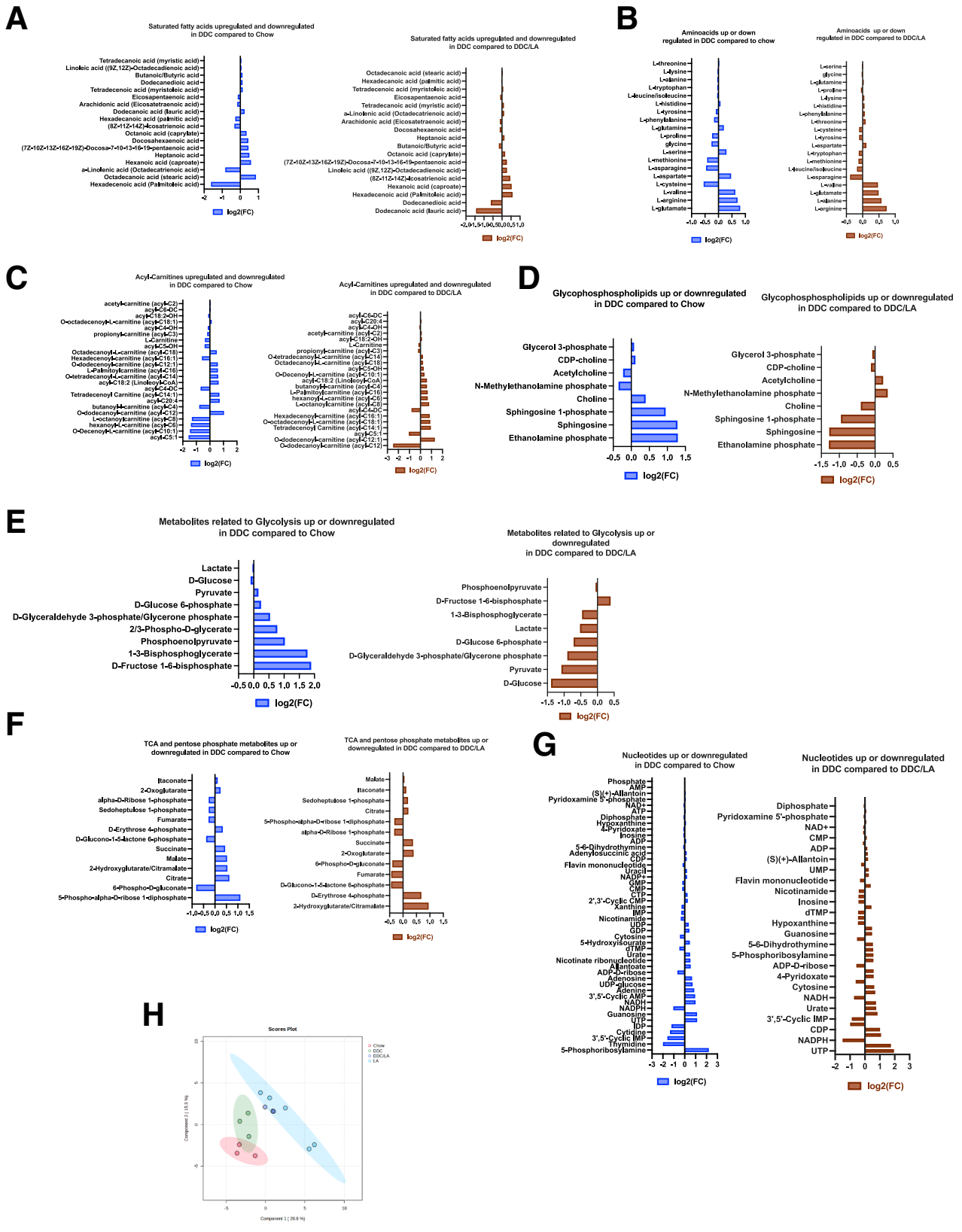
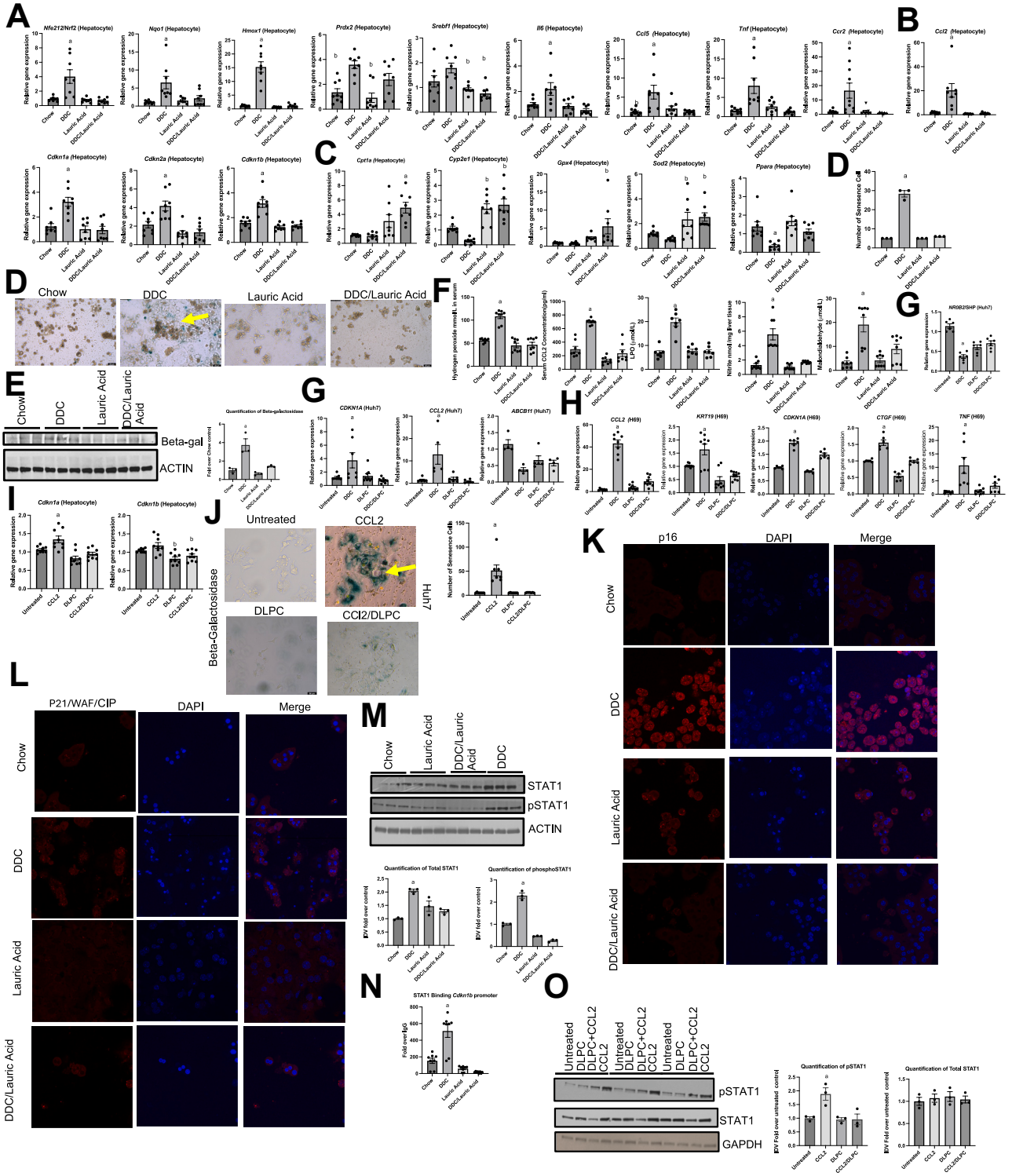


Figure 4. Effect of LA on the liver metabolomic profile in DDC mice. (*A–G*) Fold change analysis of liver tissue metabolites identified by LC-MS comparing DDC with chow and DDC with DDC/DLPC mouse groups for (*A*) saturated fatty acids, (*B*) amino acids, (*C*) acyl-carnitines, (*D*) glycophospholipids, (*E*) glycolysis metabolites, (*F*) pentose phosphate/tricarboxylic acid cycle, and (*G*) nucleotides. (*H*) PCA of liver metabolites from the liver of chow, DDC, LA, and DDC/LA mice showing significant shift of metabolites in DDC/LA vs DDC mouse liver. N = 3–4 per mouse group.

secreting pro-inflammatory cytokines, chemokine (C-C) motif ligand 2 (CCL2) production, and generating ROS. Consistent with this, we found elevated hydrogen peroxide in DDC mouse serum and lipid peroxides, nitrite, and malondialdehyde in hepatocytes, all of which were normalized in LA-treated DDC mice. (Figure 5*F*).

To determine if cholangiocyte injury promoted the hepatocyte injury and senescence in DDC mice, we performed a co-culture assay of Huh7 cells in the lower well and H69 cholangiocytes in the upper well, which were exposed overnight to 100 μM DDC, with or without 10 μM DLPC. The results showed that DDC exposure of



cholangiocytes increased the mRNA expression in Huh7 cells of pro-inflammatory *CCL2*, and *CDKNA1a*, with concomitant decrease in *NR0B2* and *ABCB11*/BSEP expression (Figure 5*G*), as well as elevated expression of *CCL2, KRT19, CTGF, TNF* and *CDKN1A* expression in H69 cells (Figure 5*H*). Importantly, these changes were reversed by DLPC treatment of H69 cells. In DDC mice, serum CCL2 protein (measured by enzyme-linked immunosorbent assay [ELISA]) was similarly elevated and suppressed by LA treatment (Figure 5*F*). Thus, we further explored the role of CCL2 in mediating these effects. CCL2 treatment overnight in cultured mouse primary hepatocytes induced the expression of senescence genes *Cdkn1a and Cdkn1b*, which were normalized by DLPC treatment (Figure 5*I*). In other experiments, Huh7 cells were exposed overnight to CCL2 with or without DLPC. β-gal staining (cell senescence) was increased in CCL2-exposed cells and significantly reduced with DLPC treatment (Figure 5*J*). We also isolated and cultured hepatocytes overnight from the 4 groups of mice and performed immunofluorescence microscopy for the senescence markers P16 and P21WAF1/CIP1. Hepatocytes from DDC mice showed evidence of increased expression of both senescence markers compared with chow controls, which was reversed by LA dietary treatment (Figure 5*K* and *L*). Taken together, these experiments support a role for cholangiocyte-derived CCL2 in promoting DDC-induced hepatocyte senescence, which was mitigated by the LA diet and its byproduct DLPC.

Signal transducer and activator of transcription 1 (STAT1) has been identified as a crucial signaling molecule that promotes cellular senescence by regulating genes involved in cell cycle arrest and contributing to the inflammatory responses commonly observed in senescent cells (Jiao et al., 2012; Majeed et al., 2023).[27,28] First, we observed upregulation of STAT1 phosphorylation (by Western blot) in hepatocytes isolated from DDC mice, which was prevented in the DDC/LA mice (Figure 5*M*). In silico analysis revealed STAT1 binding sites in the promoter region of *Cdkn1b*. Therefore, ChIP assay was performed on hepatocytes isolated from DDC mice and demonstrated significant STAT1 binding in the *Cdkn1b* promoter, which was suppressed in hepatocytes from DDC/LA mice (Figure 5*N*). Because CCL2 promotes STAT1 activation,[29] we next exposed primary mouse hepatocytes overnight to CCL2 with and without DLPC and observed that CCL2 increased activation of pSTAT1, which was reversed by DLPC (Figure 5*O*). Taken together, these findings suggest that DDC exposure of cholangiocytes induces cholangiocyte secretion of CCL2 (among other cytokines), which activates STAT1 in hepatocytes, inducing cellular senescence, which can be prevented by LA or DLPC. These data are consistent with hepatocyte senescence playing an important role in the DDC mouse model of inflammatory cholangiopathy and support the central role of the CCL2-STAT1 axis in promoting hepatocyte senescence.

LA Treatment Induces a Macrophage Phenotype Switch in DDC Mice

Hepatic macrophages have been shown to play an important role in cholestatic liver injury.[10,13,30] To

Figure 5. (***See previous page***). **Effect of lauric acid on expression of inflammation, senescence, and oxidative stress genes and biomarkers in hepatocytes isolated from experimental mouse groups.** qRT-PCR-mRNA analysis in hepatocytes isolated from chow, DDC, LA, and DDC/LA mice. (*A*) Genes involved in inflammation and oxidative stress. (*B*) Senescence genes. (*C*) Mitochondrial fatty acid oxidation and oxidative stress genes. (*D*) β-gal staining (*yellow arrow*) as a senescence marker in overnight cultured primary hepatocytes isolated from chow, DDC, LA, and DDC/ LA mice. Bar graph showing the number of senescent (β-gal$^+$) cells per microscopic field in liver sections from chow, DDC, DDC/LA, and LA groups. (*E*) Immunoblotting and quantification of β-gal in fresh hepatocytes isolated from chow, DDC, LA, and DDC/LA mice. (*F*) Serum hydrogen peroxide levels and CCL2 concentrations (ELISA), and lipid peroxides, nitrite, and malondialdehyde levels from isolated hepatocytes. (*G–H*) Co-culture of human cholangiocytes H69 (*upper wells*) and Huh7 cells was conducted. H69 cells were incubated with and without DDC overnight in the presence or absence of DLPC. (*G*) mRNA expression by qPCR was measured in Huh7 cells (*bottom wells*) for *CCL2, CDKN1A, NR0B2,* and *ABCB11* and (*H*) in H69 cells for *CCL2, CDKN1A, KRT19, CTGF,* and *TNF*. (*I*) Primary mouse hepatocytes were incubated with CCL2 in the presence or absence of DLPC overnight, and mRNA expression by qPCR was analyzed for senescence genes *Cdkn1a* and *Cdkn1b*. (*J*) β-gal staining (*yellow arrow* = senescent cells) of cultured Huh7 cells incubated with CCL2 overnight in the presence or absence of DLPC. Bar graph showing the number of senescent (β-gal$^+$) Huh7 cells after treatment with CCL2 alone or in combination with DLPC. CCL2 treatment markedly increased cellular senescence, which was inhibited by DLPC. (*K*) Confocal fluorescence microscopy of primary cultured hepatocytes from chow, DDC, LA, and DDC/LA mice stained with senescence marker P16 (*red*), and nuclear DAPI (*blue*) from showing increased senescence in DDC mouse hepatocytes, which was prevented by LA treatment. (*L*) Confocal fluorescence microscopy of primary mouse hepatocytes from chow, DDC, LA, and DDC/LA mice stained with senescence marker P21/WAF/CIP (*red*) and nuclear DAPI (*blue*) also showing increased senescence in DDC mouse hepatocytes, which was prevented by LA treatment. For (*G–I*), data points represent replicates in 3 independent experiments. For (*D* and *J*), photomicrographs are shown that are representative of 3 separate experiments. For (*K* and *L*), immunofluorescent images are shown that are representative of 3 separate experiments. (*M*) Western analysis of pSTAT1 protein, total STAT1, and actin expression in hepatocytes isolated from the mouse groups, including quantification of integrated density values (IDVs). (*N*) ChIP assay of hepatocytes isolated from mouse groups for STAT1 binding to the promoter region of *Cdkn1b* using a STAT1-specific antibody. (*O*) Western analysis of pSTAT1 protein expression in cultured primary mouse hepatocytes exposed to CCL2 overnight in the presence or absence of DLPC, including quantification of IDVs of immunoblots. Statistical analysis was performed by 1-way ANOVA with Tukey's correction for multiple comparisons. $^aP < .05$ vs all other groups; $^bP < .05$ vs DDC; $^bP < .05$ vs CCL2.

determine their role in DDC mice, we first conducted qPCR analysis of intrahepatic mononuclear cells (IHMCs) from DDC mice, examining pro-inflammatory and anti-inflammatory macrophage markers.[31] Expression of pro-inflammatory genes, *Il-1b, Itgam, Adgre1, Ly6c, Cxcl1, Cxcl2, and Ccl2, Cd80,* and *Cd86* was upregulated in DDC mouse IHMCs (Figure 6*A*), all of which were significantly reduced in DDC/LA mice, comparable to expression in chow-fed controls (Figure 6*A*). Conversely, expression of anti-inflammatory genes, *Clec4f1, Klf4, Msr1, Mrc1,* and *Il1rn,* was not induced in DDC mice but was markedly upregulated in IHMCs of DDC/LA mice (Figure 6*B*). To further assess macrophage polarization, we analyzed the Kupffer cell marker F4/80 along with inflammatory (LY6C1) and anti-inflammatory (CD206) proteins by flow cytometry across all four experimental mouse groups (Figure 6*C*). Flow cytometric analysis in DDC mice revealed increased F4/80+LY6C+ (M1) hepatic macrophage population and a mild increase in F4/80+CD206+ (M2) hepatic macrophages compared to chow controls. In DDC/LA mice relative to DDC-treated mice, there was a significant reduction in F4/80+LY6C+ and an increase in F4/80+CD206+ cells (Figure 6*C*). The increased abundance of F4/80+CD206+ cells in DDC/LA mice demonstrates an LA-induced anti-inflammatory polarization switch, which was associated with reduced liver injury.

To further explore the role of cholangiocytes in macrophage activation in this model, we performed co-culture of H69 cholangiocytes exposed to DDC in the presence or absence of DLPC overnight in the upper well and THP1 monocyte cells in the lower well. mRNA analysis demonstrated that exposure of the H69 cells to DDC led to increased expression of pro-inflammatory genes (*IL1B*) in the THP1 cells, while expression of anti-inflammatory genes (*KLF4, IL1RN*) was elevated in THP cells co-cultured with DLPC and DDC exposed H69 cells. Taken together, these data support the cholangiocyte playing a role in macrophage activation in the DDC model (Figure 6*D*) which can be mitigated by LRH-1 activation.

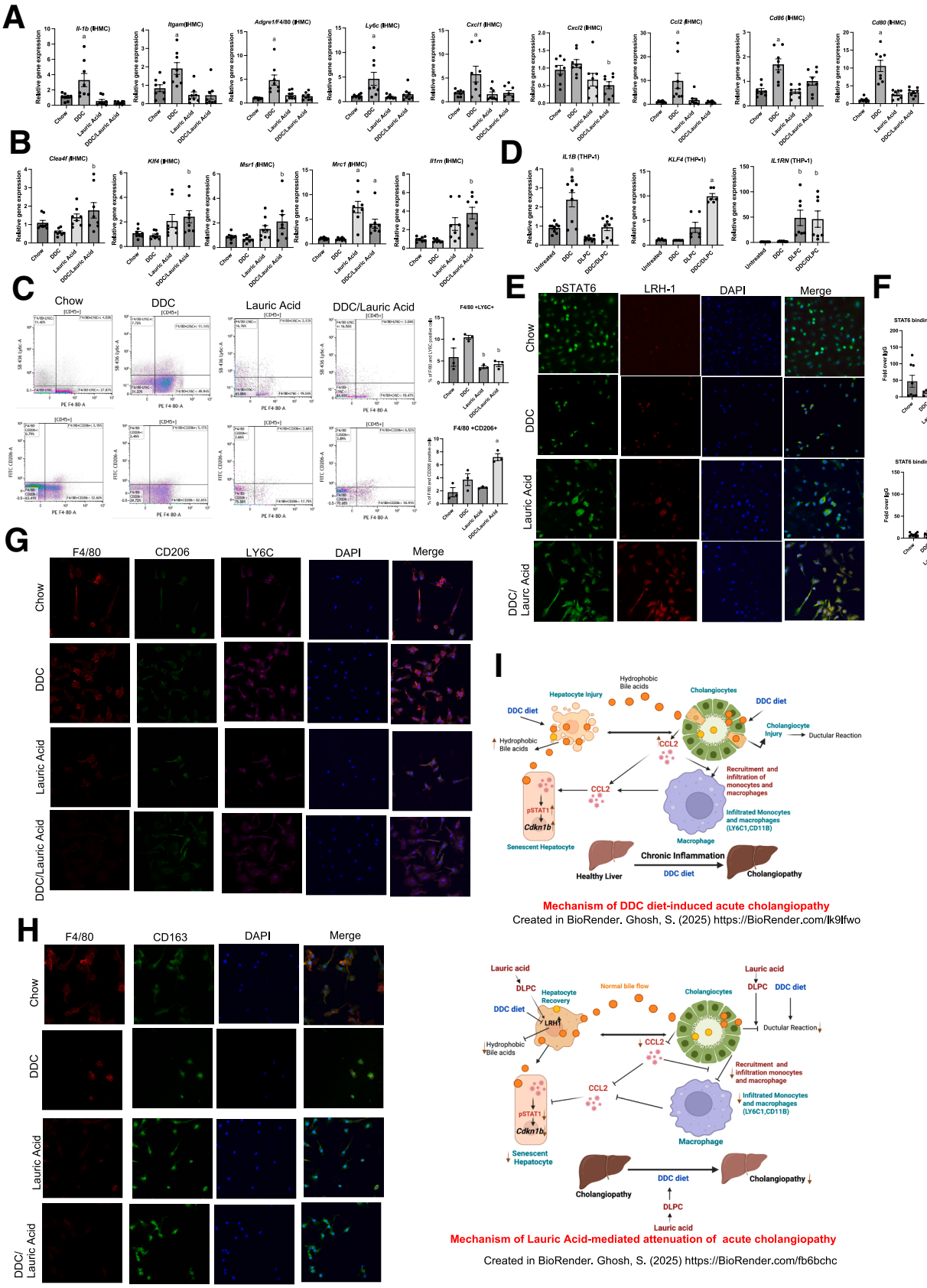
In a previous study, we demonstrated that DLPC induced anti-inflammatory STAT6 and LRH-1 signaling while inhibiting the pro-inflammatory pathway in the PNAC mouse model.[13] The upregulation of anti-inflammatory genes by LA in the DDC mouse, many of which are regulated by signal transducer and activator of transcription 6 (STAT6) signaling, suggested that STAT6 activation could be responsible for the observed phenotypic shift in macrophages, potentially linked to LRH-1.To investigate this hypothesis, we performed immunofluorescence confocal microscopy on bone marrow-derived macrophages (BMDMs) isolated from DDC/LA mice and compared them with DDC, LA, and chow-fed controls using phospho-STAT6 (p-STAT6) and LRH-1 antibodies. The results showed that LA dietary treatment was associated with increased colocalization of p-STAT6 and LRH-1 in the BMDMs of DDC mice (Figure 6*E*). ChIP assays performed to determine whether LA influenced STAT6 occupancy on the promoters of anti-inflammatory genes showed that STAT6 binding to the promoters of *Arg1* and *Chil3* was significantly enhanced in the livers of DDC/LA mice compared to DDC mice, consistent with the observed upregulation of anti-inflammatory gene expression (Figure 6*F*). Finally, in BMDMs from experimental mice, we analyzed the Kupffer cell marker F4/80 along with inflammatory (LY6C1) and anti-inflammatory (CD206) antibody staining by confocal microscopy, which demonstrated that LA treatment reduced LY6C1 positive macrophages while increasing CD206-positive cells (Figure 6*G*). We also showed that CD163 staining (an anti-inflammatory marker on macrophages) was increased in both LA and DDC/LA mice compared with chow and DDC mice (Figure 6*H*).

In summary, LA treatment significantly alters hepatic macrophage polarization in the DDC-induced mouse model. This shift is accompanied by a reduction in pro-inflammatory gene expression and an increase in anti-inflammatory markers in intrahepatic mononuclear cells. Additionally, LA treatment enhanced STAT6 and LRH-1 activation and binding to relevant anti-inflammatory gene promoters, suggesting that LA-mediated activation of STAT6 and LRH-1 plays a pivotal role in promoting macrophage polarization and resolving liver inflammation in this acute model of inflammatory cholangiopathy.

Discussion

In this study, we investigated the effects of LA and its derivative LRH-1 agonist DLPC, and the potential activation of LRH-1 pathways, on early mechanisms of liver injury and cholestasis in a 3-day DDC mouse model.[17,32] This model[17,33] was chosen because it reproduces the main histopathological hallmarks of human cholestatic diseases, including hepatocyte and biliary epithelial cell injury, ductular reaction, inflammatory macrophage infiltration, and cytokine and chemokine production. Our use of a 3-day acute DDC feeding approach was intentional to identify the earliest cellular and molecular events that could be potentially modifiable to prevent progression to a more chronic, fibrosing phase of disease.[34–39] Our results demonstrate the role of perturbations of bile acid metabolism, oxidative stress, hepatocyte senescence, and macrophage-induced inflammation in the early phase of DDC-induced cholangiopathy. Moreover, dietary supplementation with LA and DLPC led to activation of LRH-1 signaling and macrophage anti-inflammatory polarization, which were associated with prevention of DDC-induced hepatobiliary injury, as observed in other models of hepatic injury.[16,40]

Using metabolomics and molecular analyses, we elucidated key pathways through which LA modulates hepatic injury.[7,41,42] Bile acid profiling revealed significant disruptions of hepatic bile acid homeostasis in DDC mice, resulting in an accumulation of hydrophobic and conjugated bile acids.[43] DDC exposure led to suppression of bile acid synthesis gene transcription in hepatocytes compared with chow mice, which may have been a secondary protective response to mitigate the effects of elevated bile acids. The alterations in bile transporters in DDC mice are analogous


A
Il-1b (bHMC)
Itgam(bHMC)
Adgre1/F4/80 (bHMC)
Ly6c (bHMC)
Cxcl1 (bHMC)
Cxcl2 (bHMC)
Ccl2 (bHMC)
Cd86 (bHMC)
Cd80 (bHMC)
Relative gene expression
Chow
DDC
Lauric Acid
DDC/Lauric Acid
B
Cleo4f (bHMC)
Klf4 (bHMC)
Msr1 (bHMC)
Mrc1 (bHMC)
Il1rn (bHMC)
D
IL1B (THP-1)
KLF4 (THP-1)
IL1RN (THP-1)
Untreated
DDC
DLPC
DDC/DLPC
C
Chow
DDC
Lauric Acid
DDC/Lauric Acid
F4/80 +LY6C+
F4/80 +CD206+
E
pSTAT6
LRH-1
DAPI
Merge
Chow
DDC
Lauric Acid
DDC/ Laurc Acid
F
STAT6 binding to Arg1 Promoter
STAT6 binding to Chil3 Promoter
Fold over IgG
G
F4/80
CD206
LY6C
DAPI
Merge
Chow
DDC
Lauric Acid
DDC/Lauric Acid
I
Hydrophobic Bile acids
Hepatocyte Injury
Cholangiocytes
DDC diet
Cholangiocyte Injury
Ductular Reaction
CCL2
Recruitment and infiltration of monocytes and macrophages
pSTAT1
Cdkn1b
Infiltrated Monocytes and macrophages (LY6C1,CD11B)
Senescent Hepatocyte
Macrophage
Healthy Liver
Chronic Inflammation
Cholangiopathy
Mechanism of DDC diet-induced acute cholangiopathy
Created in BioRender. Ghosh, S. (2025) https://BioRender.com/lk9lfwo
H
F4/80
CD163
DAPI
Merge
Chow
DDC
Lauric Acid
DDC/ Lauric Acid
Lauric acid
DLPC
Hepatocyte Recovery
Normal bile flow
LRH1
Senescent Hepatocyte
Mechanism of Lauric Acid-mediated attenuation of acute cholangiopathy
Created in BioRender. Ghosh, S. (2025) https://BioRender.com/fb6bchc

to human chronic cholestatic conditions, such as PBC and PSC, in which canalicular bile acid transporter down-regulation is a prominent feature.[44] LA treatment also reduced hepatic levels of hydrophobic bile acids and increased hydrophilic bile acids (eg, UDCA). These LA effects were associated with upregulated mRNA expression and activation of LRH-1 and FXR signaling pathways, evidenced by increased binding of LRH-1 to promoters of fibroblast growth factor 15 (FGF15) in terminal ileum and SHP in terminal ileum and liver, increased expression of target genes (as observed in other cholestasis mouse models[12,13,45]), and upregulation of hepatocyte bile acid transporters.[46,47] LA also upregulated terminal ileal expression of LRH-1, SHP, organic solute transporter subunit beta (OST-β), and *Fgf15* while reducing ileal ASBT. The combined effect of these ileal transcriptional alterations would reduce enterocyte bile acid absorption and transport back to the liver, thus protecting the liver from undue exposure to potentially toxic bile acids.[43,48,49] The LA diet resulted in LRH-1 activation in hepatocytes, while simultaneously activating the anti-inflammatory transcription factor STAT6 to modulate macrophage polarization. This coordinated signaling resulted in reduced expression of senescence-associated markers and other pro-inflammatory cytokines.

At the cellular level, DDC-induced liver injury was characterized by macrophage polarization toward the pro-inflammatory phenotype and the promotion of hepatocyte senescence via the CCL2-STAT1 axis.[29,32,27] LA treatment (with accompanying evidence of production of DLPC) reversed these changes by shifting macrophages toward the anti-inflammatory M2 phenotype through STAT6 activation.[13] A critical aspect of DDC-induced liver injury is the induction of hepatocyte senescence via the CCL2-STAT1 axis.[28] Elevated STAT1 activation in hepatocytes isolated from DDC-treated mice was associated with increased expression of senescence markers. Mechanistically, STAT1 binding to the *Cdkn1b* promoter highlighted its role in driving senescence-related gene expression. The increased CCL2 mRNA expression in macrophages and hepatocytes from DDC mice, upregulated CCL2 expression in DDC-exposed cholangiocyte cells, and the increased serum CCL2 level in DDC mice all support a key role for this chemokine in this model. CCL2's chemoattractant activity was associated with increased infiltration of LY6C+ monocytes in the liver of DDC mice. In addition, CCL2 was likely involved in the activation of STAT1 in hepatocytes, where it induced cell senescence through binding to sites on promoters of senescence genes. All of these effects related to CCL2 were reversed by LA treatment of DDC mice or in cell cultures treated with DLPC. LRH-1 agonist, DLPC, suppressed CCL2-induced STAT1 phosphorylation and reduced senescence, indicating the role of LRH-1. These findings suggest that targeting the CCL2-STAT1 axis with LA or its derivatives could attenuate hepatocyte senescence and associated liver dysfunction in cholestatic liver diseases. Finally, LA and DLPC promoted STAT6 activation and binding to promoter sites of anti-inflammatory genes in the liver from DDC mice.

Concurrently, LA and DLPC inhibited CCL2 production in macrophages and cholangiocytes and, as a result, decreased STAT1 activation in hepatocytes and reduced senescence markers and oxidative stress.[42] Metabolomic profiling demonstrated that LA mitigated DDC-induced disruptions in hepatic amino acid, fatty acid, and energy metabolism, including reducing oxidative stress.[4,7] The shift toward short-chain acylcarnitines and restoration of mitochondrial β-oxidation pathways support LA's role in improving cellular energy homeostasis and limiting peroxide production.[50]

Metabolomics analysis of liver in the DDC mouse showed elevated levels of metabolites in a number of key hepatocyte biochemical pathways, which have been reported in other

Figure 6. (***See previous page***). **LA treatment induces an anti-inflammatory gene polarization in IHMCs and BMDMs in DDC mice.** (*A*) mRNA expression of proinflammatory genes (*Il-1b, Itgam, Adgre1, Ly6c, Cxcl1, Cxcl2, Ccl2, Cd80,* and *Cd86)* in IHMCs demonstrating activation by DDC and suppression by LA. (*B*) mRNA expression of anti-inflammatory/repair genes in IHMCs (*Clec4f, Klf4, Msr1, Mrc1*, and *Il1rn*) demonstrating induction by LA in DDC mice. (*C*) Flow cytometric analysis of IHMCs shows decreased F4/80+LY6C+ and increased F4/80+CD206+ macrophages in DDC/LA mice compared with DDC mice. (*D*) Co-culture of human H69 cholangiocytes exposed overnight to DDC with and without DLPC (*upper wells*) and human monocyte/macrophage THP-1 (*lower wells*) was conducted. *IL1B*, *KLF4,* and *IL1RN* mRNA expression was analyzed in THP-1 cells. (*E*) Confocal microscopy of immunostaining for pSTAT6 (*green*), LRH-1 (*red*), and DAPI (*blue*) in cultured BMDMs from chow, DDC, LA, and DDC/ LA mice. Colocalization of pSTAT6 and LRH-1 was demonstrated in cells from DDC/ LA mice (*yellow*). (*F*) ChIP assay examining STAT6 binding to the promoter of *Arg1* and *Chil3* was performed in liver homogenate from chow, DDC, LA, and DDC/ LA mice. (*G*) Confocal fluorescence microscopy of BMDMs isolated from mouse groups that were stained with CD206 (*green*), F4/80 (*red*), LY6C (*magenta*), and DAPI (*blue*). (*H*) Confocal fluorescence microscopy of BMDMs from mouse groups stained with F4/80 (*red*), CD163 (*green*), and DAPI (*blue*). (*I*). Proposed mechanism of DDC-induced hepatocyte and cholangiocyte injury, promoting inflammation and cholangiopathy (Created with BioRender.com). Feeding mice a DDC diet leads to the accumulation of hydrophobic bile acids and induction of inflammation, causing hepatocyte and cholangiocyte injury. Injured hepatocytes secrete CCL2 and undergo senescence, characterized by pSTAT1 activation and increased *Cdkn1b* expression. Cholangiocyte injury further amplifies CCL2 production. Elevated CCL2 recruits monocytes and macrophages ($LY6C1^{+}$) into the liver. The combined hepatocyte and cholangiocyte injury, along with macrophage infiltration and ductular reaction, drives persistent inflammation and progressive cholangiopathy. LA supplementation enhances LRH-1 signaling through DLPC, promoting hepatocyte recovery and normalization of bile acid homeostasis. This intervention reduces CCL2 production, macrophage infiltration, hepatocyte senescence, and ductular reaction, collectively attenuating cholangiopathy progression. Data are mean ± SEM. Data points represent individual mice. N = 3–8 animals per group. Statistical analysis was performed by 1-way ANOVA with Tukey's correction for multiple comparisons. $^{a}P < .05$ vs all other groups; $^{b}P < .05$ vs DDC. $^{c}P < .05$ vs chow.

liver conditions that involve inflammation, mitochondrial dysfunction, cellular senescence, and oxidative stress. These include heptanoic acid, L-arginine, palmitoyl carnitine, and the TCA cycle metabolites, succinate, 2-oxoglutarate, and citrate. Adenine and 3,5-cAMP were significantly increased in DDC mice, consistent with nucleotide imbalances associated with inflammation and mitochondrial oxidative stress.[51,52] Elevated urate in DDC mice, which responded to LA supplementation, may indicate disrupted purine or mitochondrial metabolism related to inflammation during DDC liver injury. The liver metabolomic data identifies several metabolites with known antioxidant functions that were elevated in the DDC/LA group, suggesting a protective metabolic adaptation against oxidative stress. Together, the upregulation of these metabolites supports the conclusion that LA supplementation in the context of DDC-induced cholangiopathy enhances antioxidant capacity through metabolic reprogramming, thereby reducing oxidative stress and potentially attenuating liver injury.

Our findings underscore the dual mechanisms of LA in mitigating liver injury: (1) promoting bile acid homeostasis through LRH-1 and FXR signaling; and (2) resolving inflammation and senescence through STAT6 and STAT1 modulation.

In conclusion, the results of this proof-of-principle study demonstrate that LA supplementation modulates macrophage polarization and hepatocyte senescence, with accompanying normalization of bile acid metabolism and mitochondrial gene expression, to attenuate liver injury in the early phases of DDC-induced cholangiopathy. This study demonstrates the therapeutic potential of targeting STAT6 and STAT1 pathways to restore liver homeostasis and resolve inflammation and chronic cholangiopathy (Figure 6*I*). Finally, these results indicate the plausibility of LA's therapeutic potential in inflammatory cholangiopathies, which should be pursued in more chronic cholangiopathy models.

Methods

Animal Studies

All animal procedures were approved by the Institutional Animal Care and Use Committee (IACUC) of the University of Colorado Anschutz Medical Campus. The study was conducted following the ARRIVE guidelines to ensure a rigorous and reproducible experimental design. Male C57BL/6J mice were purchased from Jackson Laboratory and housed in a standard pathogen-free barrier facility under a 12-hour light-dark cycle. Male mice were used for our experiments to avoid the effects of female hormones, specifically estrogens, on inhibition of nuclear receptor gene expression, bile formation, and bile flow which could have a confounding effect on the cholestasis in DDC mice.[53,54] Mice were provided food and water ad libitum and were acclimatized for 1 week before initiation of experiments. Eight-week-old male C57BL/6J mice were randomly assigned to the following experimental groups, with each group housed in a separate cage to minimize environmental variability and social isolation.

- **Chow (control):** Mice were fed a standard chow diet.
- **DDC:** Mice were fed a diet containing 0.1% (wt/wt) DDC (Sigma-Aldrich, Cat. No. 137030) for 3 days.
- **LA:** Mice were fed a diet supplemented with 20% LA for 3 days.
- **DDC + LA:** Mice were fed a diet containing both 0.1% (wt/wt) DDC and 20% LA for 3 days.
- **ML179:** Mice were injected i.p. with the LRH-1 inverse agonist ML179 (10 mg/kg/body weight) for 3 days.

All experimental diets were custom formulated by Inotiv Pharmaceutical Company by study specifications. All research was conducted in accordance with both the declarations of Helsinki and Istanbul.

Sample Collection

At the end of the experimental period, mice were anesthetized with i.p. pentobarbital. Blood samples (100–400 μL) were collected via the retro-orbital plexus. Liver, terminal ileum, and BMDMs were harvested and either stored at −80°C for further molecular analyses or processed for immunostaining and confocal microscopy. Serum ALT, AST, alkaline phosphatase, and total bilirubin levels were measured using coded serum samples at the University of Colorado Hospital Clinical Chemistry Laboratory. Total serum bile acids were quantified using the Total Bile Acid Assay Kit (Diazyme Laboratories, Cat. No. DZ042A-KY1) according to the manufacturer's instructions.

Primary Mouse Hepatocyte Isolation and Plating

Hepatocytes were isolated from fresh liver tissue using a modified version of previously established protocols.[13] In brief, a 24-gauge catheter was inserted into the inferior vena cava for in situ liver perfusion of anesthetized mice. The procedure involved sequential perfusion with the following buffers: (1) Earle's Balanced Salt Solution (EBSS) containing EGTA (Gibco, Cat. No. 14155) for 15 minutes; (2) liver perfusion media (Gibco, Cat. No. 17701) for 6 minutes; and (3) liver digest media with collagenase (Gibco, Cat. No. 17703) for 15 minutes at 37°C. Following perfusion, the liver tissue was excised, filtered through a 70-μm strainer, and washed with William's E media (Gibco, Cat. No. 32551). The hepatocyte pellet was obtained by centrifugation at 25 g for 5 minutes and subsequently used for primary hepatocyte culture experiments and RNA and protein extraction, as well as ChIP assay. Mouse primary hepatocytes were treated with CCL2 in the presence or absence of DLPC overnight and next day the cells were harvested for qPCR and immunoblotting.

Lipid Peroxide Assay

Lipid peroxides content was measured in isolated hepatocytes of different groups using a lipid peroxide detection kit (Elabscience, E-BC-K176-M) following the manufacturer's instructions. The optical density (OD) value at 586 nm was detected using a microplate reader.

Nitrite Assay

Nitric oxide content was measured in isolated hepatocytes of different groups using a nitrite assay kit (Millipore-Sigma Aldrich, MAK367) following the manufacturer's instructions. The OD value at 540 nm was detected using a microplate reader.

Malondialdehyde Assay

Malondialdehyde content was measured from isolated hepatocytes of different groups using a malondialdehyde detection kit (Elabscience, E-BC-K025-M) following the manufacturer's instructions. The OD value at 532 nm was detected using a microplate reader.

IHMC Isolation

Mononuclear cells were isolated from mouse liver following established protocols.[13] Briefly, liver tissue was minced in cold Hanks' buffer (Gibco/Invitrogen) and incubated with LiberaseR (Cat. No. 05989132001, Hoffman-La Roche) and DNase (Sigma-Aldrich) at 37°C for 30 minutes. The digested tissue was then filtered through a 100-μm cell strainer and subjected to low-speed centrifugation at 25 g for 3 minutes. Further filtration was performed using a 70-μm filter, followed by centrifugation at 300 g for 5 minutes. The resulting cell suspension was layered onto a 40% Histodenz gradient and centrifuged at 1500 g for 20 minutes. The mononuclear cells collected from the gradient were predominantly IHMCs.

RNA Isolation and Quantitative Gene Expression Analysis

RNA was extracted from liver homogenates, isolated primary hepatocytes, IHMCs, BMDMs, or cell line samples using TRIzol (Invitrogen) following the manufacturer's instructions, or with the QIAGEN RNeasy kit. The RNA was then used for cDNA synthesis using a kit (Cat. No. 1708891; BioRad). Real-time qPCR was performed using TaqMan probes (Thermo Fisher Scientific) as outlined in Table 3, following the method previously described.[10]

ML179 Incubation With T84 Cholangiocarcinoma Cells

T84 cells are a widely used human intestinal epithelial cell line derived from a colonic carcinoma. They are especially valuable in gastrointestinal and mucosal immunology research because they form polarized epithelial monolayers with tight junctions—closely mimicking the intestinal barrier.[55] Cultured low-passaged (NO 10–20) and 80% confluence T84 cells were exposed overnight to vehicle or 5 μM ML179 (inverse agonist) using Dulbecco's Modified Eagle Medium (DMEM)/F12 with 10% fetal bovine serum (FBS), penicillin/streptomycin media. mRNA was extracted as above, converted into cDNA, and analyzed using quantitative real-time polymerase chain reaction (qRT-PCR).

Table 3. List of TaqMan Probes

Gene	Probe set
Mouse	
Nr5a2	Mm00446088
Nr0b2	Mm00442278
Abcg5	Mm00446241
Abcg8	Mm00445980
Abcb11	Mm00445168
Abcc3	Mm00551550
Cyp7a1	Mm00484150
Cyp7b1	Mm00484157
Cyp8b1	Mm00501637
Cyp27a1	Mm00470430
Fgf15	Mm00433278
Slc10a2	Mm00488258
Slco1b2	Mm00451510
Slc51b	Mm01175040
FGFR4	Mm01341852
Nr1h4	Mm00436425
Il-1b	Mm00434228
Il1rn	Mm00446186
Clec4f	Mm00443934
Cd80	Mm00711660
Cd86	Mm00444540
Retnla	Mm00445109
Msr1	Mm00446214
Mrc1	Mm01329359
Klf4	Mm00516104
Ppara	Mm00440939
Cd163	Mm00474091
Adgre1	Mm00802529
Itgam	Mm00434455
Pparg	Mm00440940
Ccl5	Mm01302427
Ccl2	Mm00441242
Cxcl1	Mm04207460
Cxcl2	Mm00436450
Cdkn1a	Mm01303209
Cdkn1b	Mm00438168
Cdkn2a	Mm00494449
Nfe2l2	Mm00477784
Nq01	Mm01253561
Hmox1	Mm00516005
Prdx2	Mm00448996
Srebf1	Mm00550338
Il6	Mm00446190
Cyp2e1	Mm00491127
Human	
ABCG8	Hs00223690
ABCB11	Hs00994811
CDKN1A	Hs00355782
CDKN1B	Hs00153277
IL-1B	Hs01555410
IL1RN	Hs00893626
NR5A2	Hs00187067
NR0B2	Hs00222677
TNF	Hs00174128
FGF19	Hs00192780
KRT19	Hs00761767
CTGF	Hs00170014
CCL2	Hs00234140
IL6	Hs00174131

Co-culture Experiments

H69 human cholangiocyte cells were maintained in DMEM/Ham's F12 (1:1) medium supplemented with 10% defined FBS, 100 U/mL penicillin, 100 μg/mL streptomycin, 24 μg/mL adenine, 5 μg/mL insulin, 0.2 μg/mL

epinephrine, 2 nM triiodothyronine with 5 μg/mL transferrin, 10 ng/mL EGF, and 0.5 μg/mL hydrocortisone. Cells were cultured at 37°C in a humidified incubator with 5% CO_2. Medium was replaced every 2 to 3 days, and cells were passaged at approximately 80% to 85% confluence using 0.05% trypsin–EDTA. H69 cells were maintained at low passage numbers for all experiments. In trans-well co-culture experiments, H69 cells were plated on the inserts and co-cultured with either Huh7 or THP-1 human monocyte cells, which were plated in the bottom of the lower chamber in 12-well plates (Thermo Fisher Scientific). The cultured H69 cells were exposed overnight to vehicle or 100 μM DDC, either with or without 10 μM DLPC. mRNA was extracted from both cell types, converted into cDNA, and analyzed using qRT-PCR.

Immunoblot

Total cell lysates of isolated hepatocytes were prepared using M-PER and T-PER Extraction Reagents (Thermo Fisher Scientific) used following the manufacturer's guidelines. Proteins were resolved on 4-20% sodium dodecyl sulfate (SDS) polyacrylamide gels (Bio-Rad) and transferred to polyvinylidene fluoride (PVDF) membranes (EMD Millipore) for immunoblotting, following the manufacturer's protocol. All antibodies used in this study are listed in Table 4.

ChIP Assay

ChIP assays were performed on isolated mouse hepatocytes and mouse liver homogenate using the EZ ChIP/Magna ChIP G Kit (EMD/Millipore) following the manufacturer's guidelines. Specific antibodies for LRH-1 (*Abcg5/8, Nr0b2*), STAT1 (*Cdkn1b*), and STAT6 (*Arg1, Chil3*) were used, and promoter sequences from the respective genes were amplified using specific primer sets and analyzed by PCR, as previously described.[12]

β-Gal Assay

β-Gal staining was performed on overnight cultured primary hepatocytes from different mouse groups and cultured Huh7 cells using the Cellular Senescence Kit (cat. no. GXS0003; OZ Bioscience) following the manufacturer's protocol.

CCL2 ELISA

The mouse CCL2 detection assay kit (Cat: 6721, Chondrex, Inc) was employed as per the manufacturer's instructions to measure serum concentrations of CCL2.

Metabolomics and Bile Acid Analysis

To extract metabolites, homogenized liver tissue was suspended in cold 5:3:2 MeOH: ACN:H_2O (v/v/v) solution at a concentration of 15 mg/mL. Samples were then vortexed vigorously for 30 minutes at 4°C after 5 minutes of glass bead beating, then centrifuged for 10 minutes at 18,213 rcf. Using 10-uL injection volumes, the supernatants were analyzed by ultra-high-pressure-liquid chromatography coupled to mass spectrometry (UHPLC-MS; Vanquish and Exploris, Thermo). Metabolites were resolved across a 1.7 um, 2.1 × 150 mm Kinetex C18 column using a 5-minute gradient previously described.[1] Metabolomics extracts were also analyzed for bile acids using UHPLC-MS. Metabolites were resolved across a 1.7 um, 2.1 × 100 mm Acquity BEH column using a 7-minute gradient previously described.[19] Following data acquisition, .raw files were converted to .mzXML using RawConverter. Metabolites were then assigned based on intact mass, 13C isotope pattern, and retention times in conjunction with the KEGG database and an in-house standard library. Peaks were integrated using Maven (Princeton University). Quality control was assessed by using technical replicates run at the beginning, end, and middle of each sequence as previously described.[20]

Lipidomics

To extract lipids, liver tissue was suspended in cold 100% MeOH at a concentration of 15 mg/mL. Samples were then vortexed vigorously for 30 minutes at 4°C after 5 minutes of glass bead beating, then centrifuged for 10 minutes at 18,213 rcf. Using 10 uL injection volumes, the supernatants were analyzed with UHPLC-MS. Lipid metabolites were resolved across a 1.7 um, 2.1 × 150 mm

Table 4. List of Antibodies

Antibody	Catalog No.	Dilution	Vendor
LRH-1	sc-393369	1:1000	Santa Cruz Biotechnology
Beta-Galactosidase	A-11132	1:1000	ThermoFisher Scientific
P21 Waf1/Cip	2947	1:1000	Cell Signaling
Phospho-STAT1	9167	1:1000	Cell Signaling
STAT1	9172	1:1000	Cell Signaling
Phospho-STAT6	56554	1:1000	Cell Signaling
GRB2	3972	1:1000	Cell Signaling
Anti-Mouse- IgG-HRP	HAF007	1:5000	R&D Systems
Anti-Rabbit -IgG-HRP	7074	1:5000	Cell Signaling

Kinetex C18 column using a 5-minute gradient, as previously described.[21]

Histological Analysis

After sacrifice, the liver tissues were removed, fixed in formalin, embedded in paraffin, and sectioned at 10 microns. Slides were stained with H&E. For immunohistochemistry, paraffin sections were prepared for immunodetection of F4/80 (Cell Signaling; clone D2S9R; 1:200, 100 μL per slide) and Cytokeratin 19 (Proteintech; polyclonal; 1:1000, 100 μL per slide). Antigen retrieval was performed in 10 mM sodium citrate dihydrate buffer (pH 6.0) containing 0.1% Tween 20 for 10 minutes at 110°C using the NxGen Decloaker (Biocare), followed by a 10-minute ambient cool down. Immunodetection was carried out on a Discovery Ultra autostainer (Ventana/Roche) with primary antibody incubation for 32 minutes (F4/80) and 16 minutes (cytokeratin 19) at 37°C. Signal detection was performed using the OmniMAP anti-Rabbit horseradish peroxidase (HRP) and ChromoMAP 3,3′-diaminobenzidine (DAB) detection kit (Ventana/Roche) with 12-minute incubations for each reagent at 37°C. Sections were counterstained with Harris hematoxylin for 2 minutes, blued in 1% ammonium hydroxide, dehydrated through graded alcohols, cleared in xylene, and mounted with synthetic resin, all performed at the University of Colorado Cancer Center Research Histology core.[12]

Flow Cytometry

Mouse BMDMs were isolated, washed and resuspended in staining buffer (Thermo Fisher Scientific) and stained with specific antibodies, as previously described.[26] Primary antibodies were used to label cells for F4/80, Ly6C, and CD206 (Thermo Fisher Scientific). Flow-assisted cell analysis was conducted at the University of Colorado Cancer Center Flow Cytometry Core Facility and was performed on Yeti flow cytometry device (Bio-rad), and data were analyzed using Kaluza software (Beckman Coulter).

Immunostaining

BMDM or mouse primary heapatocytes cells were cultured on glass coverslips and fixed with 4% paraformaldehyde and washed with Tris-buffered saline (TBS). All reagents were diluted in TBS, and coverslips were washed by immersion into TBS between each staining step. Coverslips were incubated sequentially with 0.5% Triton-X100 (Sigma), blocking buffer (15 minutes), primary antibody diluted in blocking buffer (overnight, 4°C), and secondary antibody diluted in blocking buffer (1 hour, room temperature). Coverslips were mounted on glass slides using 4',6-diamidino-2-phenylindole (DAPI) containing ProLong Gold Antifade Mountant with DAPI mounting media (Catalog No. P36931; Thermofisher) as per manufacturer's instructions.[26] Confocal microscopy was performed on a Zeiss LSM780 spectral microscope at the University of Colorado Anschutz Medical Campus Advanced Light Microscopy Core.

Statistical Analysis

Gene expression data from qRT-PCR assays were obtained in triplicate for each mouse, and the average was calculated to determine the mean ± standard error of the mean (SEM) for gene expression in each treatment group. Each group generally included 3 to 8 animals, as indicated in the figures and legends. For cell-based experiments, gene expression was also determined in triplicate. Statistical significance was assessed using 1-way analysis of variance (ANOVA) with Tukey's correction for multiple comparisons. Differences between the 2 groups were evaluated by Student's 2-tailed unpaired student's *t*-test. A P value of $< .05$ was considered statistically significant. R/MetaboAnalyst software[56] and PRISM GraphPad software were used for statistical analyses. VIP scores were computed using the PLS-DA module in R/MetaboAnalyst software. VIP values were originated from the subjective sum of squares of the PLS-DA loadings, reflecting each metabolite's contribution to group discrimination. Model performance and robustness were assessed using software's built-in cross-validation procedures. Metabolites with VIP >1.0 are considered discriminant features and were carried forward for downstream analyses. All samples were coded and analyzed blindly, with the treatment conditions of the animals or cell lines kept unknown during analysis.

Supplementary Material

Note: To access the supplementary material accompanying this article, visit the full text version at https://doi.org/10.1016/j.jcmgh.2026.101731.

References

1. Vladut C, Ciocirlan M, Bilous D, et al. An overview on primary sclerosing cholangitis. J Clin Med 2020;9:754.
2. Banales JM, Huebert RC, Karlsen T, et al. Cholangiocyte pathobiology. Nat Rev Gastroenterol Hepatol 2019;16:269–281.
3. Zeng J, Fan J, Zhou H. Bile acid-mediated signaling in cholestatic liver diseases. Cell Biosci 2023;13:77.
4. Cai X, Tacke F, Guillot A, Liu H. Cholangiokines: undervalued modulators in the hepatic microenvironment. Front Immunol 2023;14:1192840.
5. Li M, Cai SY, Boyer JL. Mechanisms of bile acid mediated inflammation in the liver. Mol Aspects Med 2017;56:45–53.
6. Trussoni CE, LaRusso NF. Macrophages make a difference in cholestatic liver diseases - but how? J Hepatol 2023;79:1349–1351.
7. Bogert PS, O'Hara SP, LaRusso NF. Cellular senescence in the cholangiopathies. Curr Opin Gastroenterol 2022;38:121–127.
8. Trussoni CE, O'Hara SP, LaRusso NF. Cellular senescence in the cholangiopathies: a driver of immunopathology and a novel therapeutic target. Semin Immunopathol 2022;44:527–544.
9. Hong T, Chen Y, Li X, Lu Y. The role and mechanism of oxidative stress and nuclear receptors in the development of NAFLD. Oxid Med Cell Longev 2021;2021:6889533.

10. El Kasmi KC, Vue PM, Anderson AL, et al. Macrophage-derived IL-1beta/NF-kappaB signaling mediates parenteral nutrition-associated cholestasis. Nat Commun 2018;9:1393.
11. El Kasmi KC, Ghosh S, Anderson AL, et al. Pharmacologic activation of hepatic farnesoid X receptor prevents parenteral nutrition-associated cholestasis in mice. Hepatology 2022;75:252–265.
12. Ghosh S, Devereaux MW, Anderson AL, et al. NF-kappaB regulation of LRH-1 and ABCG5/8 potentiates phytosterol role in the pathogenesis of parenteral nutrition-associated cholestasis. Hepatology 2021; 74:3284–3300.
13. Ghosh S, Devereaux MW, Liu C, Sokol RJ. LRH-1 agonist DLPC through STAT6 promotes macrophage polarization and prevents parenteral nutrition-associated cholestasis in mice. Hepatology 2024; 79:986–1004.
14. Meadows V, Baiocchi L, Kundu D, et al. Biliary epithelial senescence in liver disease: there will be SASP. Front Mol Biosci 2021;8:803098.
15. Khan HU, Aamir K, Jusuf PR, et al. Lauric acid ameliorates lipopolysaccharide (LPS)-induced liver inflammation by mediating TLR4/MyD88 pathway in Sprague Dawley (SD) rats. Life Sci 2021;265:118750.
16. Sedik AA, Elgohary R, Khalifa E, et al. Lauric acid attenuates hepato-metabolic complications and molecular alterations in high-fat diet-induced nonalcoholic fatty liver disease in rats. Toxicol Mech Methods 2024; 34:454–467.
17. Pose E, Sancho-Bru P, Coll M. 3,5-diethoxycarbonyl-1, 4-dihydrocollidine diet: a rodent model in cholestasis research. Methods Mol Biol 2019;1981:249–257.
18. Sukhotnik I, Kuscuoglu U, Altindag B, et al. Intestinal involvement during 3,5-diethoxycarbonyl-1,4-dihydrocollidine-induced chronic liver injury in a mouse model. J Pediatr Surg 2011;46:1495–1502.
19. Nemkov T, Yoshida T, Nikulina M, D'Alessandro A. High-throughput metabolomics platform for the rapid data-driven development of novel additive solutions for blood storage. Front Physiol 2022;13: 833242.
20. Nemkov T, Hansen KC, D'Alessandro A. A three-minute method for high-throughput quantitative metabolomics and quantitative tracing experiments of central carbon and nitrogen pathways. Rapid Commun Mass Spectrom 2017;31:663–673.
21. Reisz JA, Zheng C, D'Alessandro A, Nemkov T. Untargeted and semi-targeted lipid analysis of biological samples using mass spectrometry-based metabolomics. Methods Mol Biol 2019;1978:121–135.
22. Ding L, Yang L, Wang Z, Huang W. Bile acid nuclear receptor FXR and digestive system diseases. Acta Pharm Sin B 2015;5:135–144.
23. Song L, Hou Y, Xu D, et al. Hepatic FXR-FGF4 is required for bile acid homeostasis via an FGFR4-LRH-1 signal node under cholestatic stress. Cell Metab 2025; 37:104–120.e109.
24. Vagnerova K, Hudcovic T, Vodicka M, et al. The effect of oral butyrate on colonic short-chain fatty acid transporters and receptors depends on microbial status. Front Pharmacol 2024;15:1341333.
25. Ghosh S, Devereaux MW, Anderson AL, et al. Stat3 role in the protective effect of FXR Agonist in parenteral nutrition-associated cholestasis. Hepatol Commun 2023;7:e0056.
26. Ghosh S, Devereaux MW, Orlicky DJ, Sokol RJ. Pharmacologic inhibition of HNF4alpha prevents parenteral nutrition associated cholestasis in mice. Sci Rep 2023; 13:7752.
27. Majeed Y, Madani AY, Altamimi AI, et al. STAT1- and NFAT-independent amplification of purinoceptor function integrates cellular senescence with interleukin-6 production in preadipocytes. Br J Pharmacol 2023; 180:609–627.
28. Jiao S, Meng F, Zhang J, et al. STAT1 mediates cellular senescence induced by angiotensin II and H(2)O(2) in human glomerular mesangial cells. Mol Cell Biochem 2012;365:9–17.
29. Yang L, Li N, Yang D, et al. CCL2 regulation of MST1-mTOR-STAT1 signaling axis controls BCR signaling and B-cell differentiation. Cell Death Differ 2021; 28:2616–2633.
30. Shan Z, Ju C. Hepatic macrophages in liver injury. Front Immunol 2020;11:322.
31. Wang N, Liang H, Zen K. Molecular mechanisms that influence the macrophage m1-m2 polarization balance. Front Immunol 2014;5:614.
32. Bruneau A, Guillot A, Tacke F. Macrophages in cholangiopathies. Curr Opin Gastroenterol 2022; 38:114–120.
33. Fickert P, Stoger U, Fuchsbichler A, et al. A new xenobiotic-induced mouse model of sclerosing cholangitis and biliary fibrosis. Am J Pathol 2007; 171:525–536.
34. Hefler J, Marfil-Garza BA, Pawlick RL, et al. Preclinical models of acute liver failure: a comprehensive review. PeerJ 2021;9:e12579.
35. Allison R, Guraka A, Shawa IT, et al. Drug induced liver injury - a 2023 update. J Toxicol Environ Health B Crit Rev 2023;26:442–467.
36. Lai Q, Angelico R, Guglielmo N, et al. Ex-situ normothermic machine perfusion prevents ischemic cholangiopathy after liver transplantation: a meta-regression analysis. Transplant Rev (Orlando) 2025; 39:100915.
37. Hashimoto Y, Miyagaki A. Peroral cholangioscopic findings of acute ischemic cholangiopathy caused by transarterial chemoembolization. Gastrointest Endosc 2023;97:990–991.
38. Liu Z, Sakamoto T, Yokomuro S, et al. Acute obstructive cholangiopathy in interleukin-6 deficient mice: compensation by leukemia inhibitory factor (LIF) suggests importance of gp-130 signaling in the ductular reaction. Liver 2000;20:114–124.
39. Grabner A. [Case report. Cholangiopathy and cholelithiasis and acute hepatic syndrome]. Tierarztl Prax 1997;25:317, 370–312.
40. Sasaki M, Miyakoshi M, Sato Y, Nakanuma Y. Chemokine-chemokine receptor CCL2-CCR2 and

CX3CL1-CX3CR1 axis may play a role in the aggravated inflammation in primary biliary cirrhosis. Dig Dis Sci 2014;59:358–364.
41. Namachivayam A, Valsala Gopalakrishnan A. Effect of Lauric acid against ethanol-induced hepatotoxicity by modulating oxidative stress/apoptosis signalling and HNF4alpha in Wistar albino rats. Heliyon 2023;9:e21267.
42. Shaheryar ZA, Khan MA, Hameed H, et al. Lauric acid provides neuroprotection against oxidative stress in mouse model of hyperglycaemic stroke. Eur J Pharmacol 2023;956:175990.
43. Li T, Hasan MN, Gu L. Bile acids regulation of cellular stress responses in liver physiology and diseases. eGastroenterology 2024;2:e100074.
44. Fiorucci S, Urbani G, Di Giorgio C, et al. Bile acids-based therapies for primary sclerosing cholangitis: current landscape and future developments. Cells 2024; 13:1650.
45. Fernandez-Marcos PJ, Auwerx J, Schoonjans K. Emerging actions of the nuclear receptor LRH-1 in the gut. Biochim Biophys Acta 2011;1812:947–955.
46. Ethanic M, Stanimirov B, Pavlovic N, et al. Pharmacological applications of bile acids and their derivatives in the treatment of metabolic syndrome. Front Pharmacol 2018;9:1382.
47. Goodwin B, Jones SA, Price RR, et al. A regulatory cascade of the nuclear receptors FXR, SHP-1, and LRH-1 represses bile acid biosynthesis. Mol Cell 2000; 6:517–526.
48. Bragazzi MC, Venere R, Vignone A, et al. Role of the gut-liver axis in the pathobiology of cholangiopathies: basic and clinical evidence. Int J Mol Sci 2023;24:6660.
49. Dawson PA, Karpen SJ. Intestinal transport and metabolism of bile acids. J Lipid Res 2015;56:1085–1099.
50. Li DK, Smith LE, Rookyard AW, et al. Multi-omics of a pre-clinical model of diabetic cardiomyopathy reveals increased fatty acid supply impacts mitochondrial metabolic selectivity. J Mol Cell Cardiol 2022; 164:92–109.
51. Misrani A, Tabassum S, Yang L. Mitochondrial dysfunction and oxidative stress in Alzheimer's disease. Front Aging Neurosci 2021;13:617588.
52. Dewanjee S, Chakraborty P, Bhattacharya H, et al. Altered glucose metabolism in Alzheimer's disease: Role of mitochondrial dysfunction and oxidative stress. Free Radic Biol Med 2022;193:134–157.
53. Papacleovoulou G, Abu-Hayyeh S, Williamson C. Nuclear receptor-driven alterations in bile acid and lipid metabolic pathways during gestation. Biochim Biophys Acta 2011;1812:879–887.
54. Chen J, Zhao KN, Liu GB. Estrogen-induced cholestasis: pathogenesis and therapeuticimplications. Hepatogastroenterology 2013;60:1289–1296.
55. Navabi N, McGuckin MA, Linden SK. Gastrointestinal cell lines form polarized epithelia with an adherent mucus layer when cultured in semi-wet interfaces with mechanical stimulation. PLoS One 2013;8: e68761.
56. Pang Z, Lu Y, Zhou G, et al. MetaboAnalyst 6.0: towards a unified platform for metabolomics data processing, analysis and interpretation. Nucleic Acids Res 2024; 52:W398–W406.

Received July 24, 2025. Accepted January 12, 2026.

Correspondence
Address correspondence to: Swati Ghosh, PhD, Department of Pediatrics, University of Colorado School of Medicine, Section of Gastroenterology, Hepatology, and Nutrition, University of Colorado-Denver Anschutz Medical Campus, 12700 E 19th Ave, P15-6450A, Aurora, Colorado 80045 e-mail: swati.ghosh@cuanschutz.edu.

Acknowledgments
The T84 cell line was a kind gift of Dr Sean Colgan, University of Colorado Anschutz Medical Campus, and the H69 cell line is a kind gift of Dr Robert C. Huebert, Mayo Clinic, Rochester, Minnesota. The authors gratefully acknowledge E. Erin Smith, HTL(ASCP)CM, and Helen DuBois, HTL(ASCP)CM, of the University of Colorado Anschutz Medical Campus, Pathology Shared Resource, Research Histology Laboratory. This core facility is supported in part by the Cancer Center Support Grant (P30CA046934). The content is solely the responsibility of the authors and does not necessarily represent the official views of the National Institutes of Health.

CRediT Authorship Contributions
Swati Ghosh, PhD (Conceptualization: Lead; Data curation: Lead; Formal analysis: Lead; Funding acquisition: Lead; Investigation: Lead; Methodology: Lead; Project administration: Lead; Software: Lead; Supervision: Lead; Validation: Lead; Visualization: Lead; Writing – original draft: Lead; Writing – review & editing: Lead)
Michael W. Devereaux, BS (Methodology: Supporting)
Aimee L. Anderson, BS (Methodology: Supporting)
Colin C. Anderson, PhD (Data curation: Supporting; Formal analysis: Supporting)
Angelo D'Alessandro, PhD (Formal analysis: Supporting; Methodology: Supporting)
David J. Orlicky, PhD (Formal analysis: Supporting)
Ronald J. Sokol (Funding acquisition: Equal; Writing – review & editing:Supporting)

Conflicts of interest
This author discloses the following: Ronald J. Sokol consults with Ipsen/Albireo, Mirum, Mallinckrodt, Astellas, and ProQR. The remaining authors disclose no conflicts.

Funding
This research was funded in part by a pilot grant from the Childhood Liver Disease Research Network, supported by the National Institute of Diabetes and Digestive and Kidney Diseases of the National Institutes of Health, grant number U01 DK062453. The content is solely the responsibility of the authors and does not necessarily represent the official views of the National Institutes of Health.

Data Availability
Data will be made available upon request.